Science of the Total Environment 769 (2021) 145157

Contents lists available at ScienceDirect

Science of the Total Environment

journal homepage: www.elsevier.com/locate/scitotenv

Effects of reduced shoreline erosion on Chesapeake Bay water clarity

Jessica S. Turner *, Pierre St-Laurent, Marjorie A.M. Friedrichs, Carl T. Friedrichs

Virginia Institute of Marine Science, William & Mary, Gloucester Point, VA 23062, USA

HIGHLIGHTS

- 3D numerical model was used to study impact of shoreline erosion on water clarity.
- Armored shorelines reduce suspended sediment, improving clarity measured by K_d^{-1}.
- Stronger effect of erosion in lower Bay and dry years due to lower river influence.
- Armored shorelines reduce inorganics, yet can increase organic matter production.
- With less erosion, extent of shallower Z_{SD} yet deeper K_d^{-1} yields Organic Fog Zone.

GRAPHICAL ABSTRACT

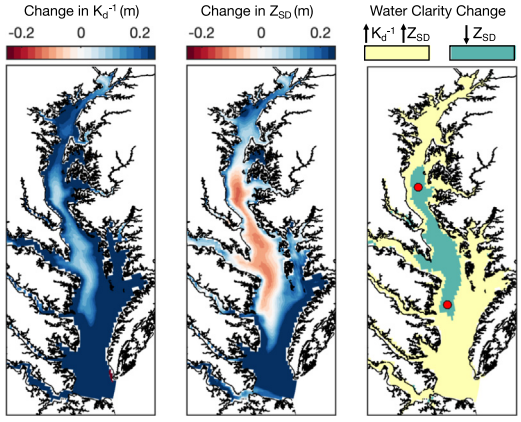

ARTICLE INFO

Article history:
Received 30 October 2020
Accepted 6 January 2021
Available online 14 January 2021

Editor: José Virgílio Cruz

Keywords:
Light attenuation
Shoreline armoring
Estuaries
Secchi depth
Suspended sediments
Shoreline erosion

ABSTRACT

Shoreline erosion supplies sediments to estuaries and coastal waters, influencing water clarity and primary production. Globally, shoreline erosion sediment inputs are changing with anthropogenic alteration of coastlines in populated regions. Chesapeake Bay, a prime example of such a system where shoreline erosion accounts for a large proportion of sediments entering the estuary, serves here as a case study for investigating the effects of changing sediment inputs on water clarity. Long-term increases in shoreline armoring have contributed to decreased erosional sediment inputs to the estuary, changing the composition of suspended particles in surface waters. This study examined the impact of shoreline erosion on water clarity using a coupled hydrodynamic-biogeochemical model. Experiments were conducted to simulate realistic shoreline conditions representative of the early 2000s, increased shoreline erosion, and highly armored shorelines. Together, reduced shoreline erosion and the corresponding reduced rates of resuspension result in decreased concentrations of inorganic particles, improving water clarity particularly in the lower Bay and in dry years where and when riverine sediment influence is low. This clarity improvement relaxed light limitation, which increased organic matter production. Differences between the two extreme experiments revealed that in the mid-estuary in February to April, surface inorganic suspended sediment concentrations decreased 3–7 mg L^{-1}, while organic suspended solids increased 1–3 mg L^{-1}. The resulting increase in the organic-to-inorganic ratio often had opposite effects on clarity according to different metrics, improving clarity in mid-Bay central channel waters in terms of light attenuation depth, but simultaneously degrading clarity in terms of Secchi depth because the resulting increase in organic suspended solids decreased the water's transparency. This incongruous water clarity effect, the spatial extent of which is defined here as an Organic Fog Zone, was present in February to April in all years studied, but occurred farther south in wet years.

* Corresponding author.
E-mail address: jsturner@vims.edu (J.S. Turner).

https://doi.org/10.1016/j.scitotenv.2021.145157

1. Introduction

Quantifying changing water clarity is important to understanding aquatic ecology and managing water quality. Water clarity exerts a key control on the functioning of aquatic ecosystems in oceanic and coastal waters worldwide because it determines the amount of light energy accessible for underwater photosynthesis. Water clarity holds great importance in coastal and estuarine waters, because of the large human populations, economically important fisheries, and linked watershed-ocean processes that characterize coastal systems. While many metrics are used to describe water clarity in aquatic environments, the present study focuses on water clarity measured by light attenuation depth (K_d^{-1}) and Secchi depth (Z_{SD}; see Appendix A for acronym definitions). K_d^{-1} is the inverse of the diffuse light attenuation coefficient K_d, which describes the logarithmic slope of the reduction in the intensity of photosynthetically active radiation (PAR) with depth (Kirk, 1994). K_d^{-1} is most closely related to overall underwater illumination and the availability of energy for autotrophs. In contrast, Z_{SD} is the depth at which a white or black and white disk can no longer be seen by the human eye (Holmes, 1970; Preisendorfer, 1986; Secchi and Cialdi, 1866; Tyler, 1968). Z_{SD}, representing image attenuation, is a measure of transparency or visibility. Over the past century, Z_{SD} has been widely used as a water clarity metric, in part because of its extreme ease of use. Trends in Z_{SD} in water bodies often reflect large-scale drivers of change, ranging from external watershed change (Jassby et al., 2003) to internal regime shifts (Effler et al., 2008). Gradually shallowing Z_{SD} has been seen in many coastal waters due to eutrophication of coastal environments. For example, trends of decreasing (i.e., shallowing) Z_{SD} have been documented in the Adriatic Sea (Justić, 1988), the Bohai Sea (Shang et al., 2016), and parts of the Baltic Sea (Bonsdorff et al., 1997; Fleming-Lehtinen and Laamanen, 2012; Harvey et al., 2019). In contrast, increasing light penetration has been documented in the Pearl River Estuary (Wang et al., 2018) and in San Francisco Bay (Cloern and Jassby, 2012) in association with reduced sediment input.

Chesapeake Bay serves as an excellent case-study estuary for water clarity change due to its turbid yet variable water clarity conditions, ecological and human relevance of water clarity in the region, and somewhat ambiguous response to watershed management efforts in recent decades. The Chesapeake Bay is a large, eutrophic estuary characterized by relatively low water clarity, i.e., shallow K_d^{-1} (strong light attenuation) and shallow Z_{SD} (low transparency), with long-term means of 1.7 m and 1.5 m, respectively, in the mainstem Bay. Water clarity conditions vary widely across spatial, seasonal, and interannual-hydrological gradients. Clarity in this estuary is a key control on timing of seasonal phytoplankton blooms and subsequent deep channel hypoxia, and clarity holds additional importance to recreation, aquaculture, fisheries, and submerged aquatic vegetation; the latter provides habitat for juveniles of commercially important species (Jones, 2014; Peterson et al., 2000; Schaffler et al., 2013). Following historical land-use change and extreme eutrophication, improved watershed management practices have been instated since the 1980s (Lefcheck et al., 2018; Zhang et al., 2018). However, the overall response of water clarity over the last 40 years has been ambiguous. Trends reveal shallowing Z_{SD} (i.e., decreased transparency) since the 1980s (Gallegos et al., 2011; Testa et al., 2019), yet at the same time, reductions in total suspended solids (TSS) and deepening K_d^{-1} (i.e., increased light penetration) (Harding et al., 2016). The mechanisms driving these opposing trends in K_d^{-1} and Z_{SD} are not yet well understood, and motivate the study described here.

Meanwhile, sediment inputs from shoreline erosion in Chesapeake Bay are decreasing as the shoreline is gradually hardened by human development (Gittman et al., 2015; Halka et al., 2006; Hardaway and Byrne, 1999; Isdell, 2014; Patrick et al., 2014; Russ and Palinkas, 2020). For sheltered coasts within the Chesapeake Bay and its tidal tributaries, approximately 25–50% of previously natural shorelines have been hardened, depending on location (Gittman et al., 2015; Patrick et al., 2016). Regional shoreline erosion adds slightly more sediment to the Bay than the two largest rivers combined (Table S1), and in the mainstem mid- to lower-=Bay shoreline erosion is the largest single source of inorganic solids (Cerco et al., 2013). Hardened shorelines have also been associated with changes in seabed grain size via deposition of finer material on landward sides of structures (Martin et al., 2005) and coarsening of the surrounding seabed (Davenport, 2012), which alters the erodibility of seabed sediments. As shorelines have been hardened, much focus has been placed on the consequences to organisms in the nearshore environment and localized ecological impacts (Bilkovic et al., 2019; Chhor et al., 2020; Patrick et al., 2016; Prosser et al., 2017). However, large-scale consequences of these decreased sediment inputs for estuary-scale biogeochemistry and water clarity have not yet been investigated.

Reductions in sediment inputs to aquatic ecosystems through shoreline hardening can alter suspended particle composition, influencing water clarity trends. Changing concentrations of inorganic mineral sediments shift the organic-to-inorganic ratio of suspended particles. For example, with higher sediment inputs, the organic-to-inorganic ratio of suspended solids decreases, and with lower sediment inputs, the organic fraction increases. The organic fraction of suspended solids has ramifications for water transparency because Z_{SD} is more sensitive to light scattering by some particle types than K_d^{-1} (Gallegos et al., 2011; Hou et al., 2007). For example, in lakes, reservoirs, and coastal bays, particulate scattering is strongly inversely correlated to Z_{SD}, and organic detrital particles often dominate contributions to Z_{SD} significantly more than to K_d^{-1} (Armengol et al., 2003; Effler and Peng, 2012; Hernádez and Gocke, 1988). The relationship between Z_{SD} and K_d^{-1} in turbid water is not fixed, since in the presence of highly-scattering particles, Z_{SD} is shallower than could be predicted by a linear relationship with K_d^{-1} (Kirk, 1994; Koenings and Edmundson, 1991). Furthermore, in extremely turbid waters, the trend reverses such that Z_{SD} is deeper than a linear trend with K_d^{-1} would predict (Bowers et al., 2020). In short, Z_{SD} and K_d^{-1} have a complex relationship that varies with the concentration and composition of suspended particles. Increased scattering due to changing amounts of organic detritus could help to explain the observed opposing trends in Z_{SD} and K_d^{-1} in Chesapeake Bay (Gallegos et al., 2011). Yet, the mechanism for a compositional change in particles, i.e., the driver of this changing organic-to-inorganic ratio, has not been clearly identified.

The primary goal of the current study is to evaluate the estuary-wide impacts of shoreline armoring on water clarity in Chesapeake Bay and to relate these impacts to the opposing trends previously documented in attenuation depth and Secchi depth. This research builds on past work by using a comprehensive modeling framework to conduct experiments to test the impact of changes in coastal erosion as possible mechanisms for complex water clarity change, taking into account the entire estuarine ecosystem. The present study seeks to answer the research question: how does a decrease in shoreline erosion associated with increased shoreline armoring affect water clarity in Chesapeake Bay? We find that shoreline armoring (reduced shoreline erosion) improves water clarity throughout the Bay in terms of K_d^{-1}, especially at locations and times with relatively low river influence, yet has spatially, seasonally, and interannually diverse impacts on Z_{SD} due to a relaxation of light limitation on organic matter production.

2. Methods

2.1. Observations: in situ data

In situ data from the Chesapeake Bay Program (CBP) Water Quality Database (Environmental Protection Agency (EPA), 2012) were used for the development of empirical equations to describe water clarity and to evaluate model skill. Associated observations have been collected on monitoring sampling cruises throughout the Bay since 1984. Timing of cruises is typically monthly during November to February and fortnightly during March to October. The present study used data from 33

mainstem stations, including the central channel and additional mainstem stations closer to shorelines and tributary river mouths (Fig. 1). Stations had water column depths of 5 to 35 m depending on location. For development of empirical equations (see Section 2.2.4), the timeframe January 1998 to December 2019 was used to avoid potential TSS biases associated with a methodology change in Virginia waters in the mid-1990s (Williams et al., 2010). Data used to develop the empirical equation for light attenuation (K_d) included surface (<2 m) salinity, TSS, and K_d sampled on the same days at the same stations ($N_{obs} = 10835$). Data used to develop the empirical equation for Z_{SD} included surface volatile suspended solids (VSS), K_d, and Z_{SD} sampled concurrently ($N_{obs} = 5046$). VSS and fixed suspended solids (FSS) are used here as proxies for organic and inorganic solids because observations of VSS and FSS are reported by the CBP Database. Data used for model skill assessment included temperature, salinity, K_d^{-1} and Z_{SD}, as well as suspended solids (TSS, FSS, and VSS, where T, F, and V indicate total, fixed, and volatile components.) Components of TSS were measured using bottle samples, 0.7-micron glass-fiber filters, drying at 103-105 °C, and combustion at 550 °C to calculate mass with and without volatilized components. When only FSS or VSS data were reported alongside corresponding TSS data, the missing component was calculated assuming TSS = FSS + VSS. In situ K_d was estimated by lowering a quanta light meter through the water column to record photosynthetically active radiation (PAR) at a series of depths from just below the surface to the depth of the 10% light level ($Z_{10\%}$), and computing the reduction in PAR relative to the surface measurement:

$$K_d = \frac{ln\left(PAR_{surface} - PAR_Z\right)}{Z_{10\%}} \quad (1)$$

PAR was also measured simultaneously in air to account for variability in incident light due to cloud cover. The observed attenuation depth (K_d^{-1}) in meters was then calculated as the inverse of observed K_d.

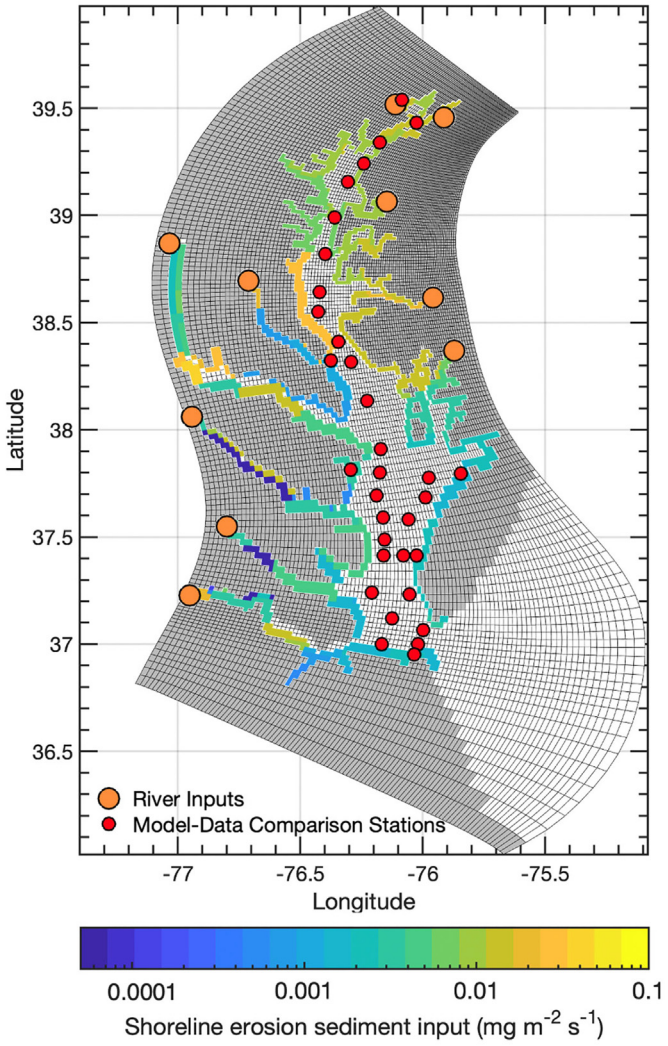

Fig. 1. Model grid, with large orange circles indicating the locations of river inputs and small red markers indicating locations of long-term monitoring stations used for model-data comparison. Colorbar indicates surface flux of total sediment mass (mg m^{-2} s^{-1}) as the mean daily flux from shoreline erosion inputs.

2.2. Estuarine model

2.2.1. Coupled hydrodynamic-biogeochemistry model

The Chesapeake Bay Estuarine Carbon and Biogeochemistry Model (ChesROMS-ECB) was used to simulate linked watershed-estuarine processes. The hydrodynamic model used in this study was an implementation of the Regional Ocean Modeling System (ROMS) (Shchepetkin and McWilliams, 2005) designed for the Chesapeake Bay (Xu et al., 2012) with a horizontal grid cell resolution of ~1.8 km (Fig. 1) and 20 terrain-following vertical levels stretched for increased depth resolution in surface waters and near the seabed. As in previous ChesROMS-ECB implementations, state variables simulated within this framework included dissolved organic and inorganic nutrients (nitrogen and carbon), oxygen, phytoplankton, zooplankton, detritus, and inorganic suspended sediments (see St-Laurent et al. (2020) supplementary information for biogeochemical equations). Terrestrial inputs of freshwater, temperature, particulate and dissolved nitrogen, and inorganic sediments were obtained from the Phase 6 CBP Watershed Model (Easton et al., 2017; Shenk and Linker, 2013), while terrestrial inputs of inorganic and organic carbon were obtained from the Dynamic Land Ecosystem model (Tian et al., 2015). As in Irby and Friedrichs (2019), inputs of particulate organic matter were divided into phytoplankton and small detritus, and dissolved organic matter was partitioned into semi-labile and refractory components. All terrestrial inputs were added at ten point-source locations in the model grid (Fig. 1), representing both overland and riverine flow.

Atmospheric forcing from the ERA5 data reanalysis product (Copernicus Climate Change Service C3S, 2017) included wind, humidity, precipitation, air temperature and pressure, and incoming longwave and net shortwave radiation. Atmospheric nitrogen deposition was also included (Da et al., 2018). Sea surface height was forced using observed non-tidal water levels from Lewes, DE and Duck, NC, along with Advanced Circulation model tidal harmonics (Luettich et al., 1992). Open ocean boundary conditions for temperature and salinity were calculated from observed vertical profiles from the World Ocean Database (Boyer et al., 2018) with climatologies derived from multiple years and long-term trends 1985–2018 applied such that temperature and salinity at the boundary varied both seasonally and interannually (Garcia and Gordon, 1992). With a similar setup to the one described here, ChesROMS-ECB has previously been used to investigate broad-scale impacts of water clarity on temperature (Kim et al., 2020), effects of resuspension on sediment and water biogeochemistry (Moriarty et al., 2021), and impacts of atmospheric deposition (Da et al., 2018), watershed management actions, and climate change on hypoxia (Irby et al., 2018; Irby and Friedrichs, 2019) and inorganic carbon balance (St-Laurent et al., 2020).

2.2.2. Sediment transport model

Most aspects of the sediment transport model implemented in the present study were consistent with those described in Moriarty et al. (2021). Specifically, three fine-grained sediment size classes were simulated with settling velocities typical of silt-rich flocs, clay-rich flocs, and unaggregated mud (Table 1), consistent with Cerco et al. (2010, 2013). Sediment concentrations in the water column were governed by shear stress dependent resuspension and deposition according to the bottom boundary layer formulation of Madsen (1994). The seabed

Table 1
Characteristics of modeled inorganic particle components of FSS and detrital components of VSS.

Type	Name	$\tau_{crit(E,D)}$ (Pa)	W_s (mm s^{-1})	Shoreline erosion input flux (kg s^{-1})	Riverine input flux (kg s^{-1})
FSS	Sand[a]	20	n.a.	0	0
	Silt-rich flocs	0.09	0.1	25.5	64.7
	Clay-rich flocs	0.09	0.03	19.1	177.1
	Unaggregated mud	0.09	0.012	19.1	9.94
VSS	Small detritus[b]	0.01	0.001	0	16.8[c]
	Large detritus[b]	0.01	0.06	0	0

[a] Sand is present in the seabed only to allow armoring to limit mud resuspension and is effectively never resuspended.
[b] From Peterson (1999).
[c] Riverine input concentrations of organic particles in kg m^{-3} were computed from carbon concentration in mmol C m^{-3} using DW:carbon ratio of 2.9.

(Fig. S1) was characterized by a spatially explicit initial grain size distribution based on observations over multiple summer seasons (Nichols et al., 1991). Wind-driven waves were implemented using output from the Simulating Waves Nearshore (SWAN) model (Booij et al., 1999) through one-way coupling to the hydrodynamics and sediment routines. Spatial patterns in the resulting current- and wave-induced bed stresses governing resuspension from the seabed (Fig. S2) reveal a strong influence of waves in the lower Bay and a strong influence of currents in the deep mainstem channel. For all four classes of inorganic particles, a seabed erosion rate of 3×10^{-5} kg m^{-2} s^{-1} was used. Finally, critical shear stress values for erosion and deposition ($\tau_{crit(E,D)}$) of sand were set to 20 Pa (Table 1), the role of sand being to armor the seabed and allow winnowing of fine sediment without the sand being resuspended (Harris et al., 2008).

To achieve the goals of the present study, the model configuration deviated from Moriarty et al. (2021) in the use of fewer seabed layers, seabed nudging toward observed grain size spatial distribution, higher critical shear stresses for fine sediment classes, and simplified seabed-water column biogeochemical setup. The seabed was initialized with two bed layers of thickness 0.5 cm and 100 cm and with the observed seabed fractions given by Nichols et al. (1991). A sediment bed porosity of 0.9 and grain densities of 2650, 2000, 1350 and 1350 kg m^{-3} were assumed for the four sediment size classes. These parameters together defined the mass of each sediment size class in the initial condition of the seabed. Through the course of the calculation, the mass of each sediment class in the seabed was slowly nudged toward this initial condition on a one-month timescale. This nudging scheme was added to reflect higher confidence in the observed grain size distribution conditions than in modeled seabed drift, while still allowing for dynamic resuspension and deposition of sediments between water column and seabed over time. Values for $\tau_{crit(E,D)}$ were set to 0.09 Pa (Table 1) for the three fine sediment classes, which allowed the model to most closely represent observed conditions. This $\tau_{crit(E,D)}$ value of 0.09 Pa, although higher than Moriarty et al. (2021) and Cerco et al. (2010, 2013), compares well with the values presented in Wu et al. (2018), Sanford and Maa (2001), and Maa et al. (1998). The $\tau_{crit(E,D)}$ parameter for fine sediment classes was altered for each of the two experimental model runs (see Section 2.3.2). Lastly, seabed-water column biogeochemical interactions in the present study were distinct from Moriarty et al. (2021) and instead consistent with Da et al. (2018) and St-Laurent et al. (2020). For example, an organic critical shear stress of 0.01 Pa (based on Peterson, 1999; Table 1) yielded results consistent with observations, characterizing the observed lower density of organic particles. As in these earlier studies, when sinking organic matter reached the seabed a fraction was resuspended as small detritus as a function of the organic matter critical shear stress, a fraction was removed via burial, and a fraction was instantly remineralized (Druon et al., 2010; St-Laurent et al., 2020).

Shoreline erosion sediment inputs, not considered in any previous ChesROMS-ECB applications, were calculated for each stretch of shoreline on an annual basis following the methodology used in the Phase 6 CBP Watershed Model (Easton et al., 2017; Shenk and Linker, 2013). Eroded sediment mass was calculated from observed long-term shoreline migration from the late twentieth century measured in aerial imagery converted to mass inputs based on observed bank sediment grain size distributions (Cerco and Noel, 2017; Halka et al., 2006; Hardaway et al., 2017). Nutrient fluxes and organic matter inputs from shoreline erosion were not considered in the current study, as bank sediments are nitrogen-poor and contain recalcitrant organic material (Johnson et al., 2018). The total amount of shoreline sediment inputs to the Bay each year was assumed to remain constant, yet within each year, inputs varied daily as a function of the wave power adjacent to each shoreline segment. In this way, the inputs were highly correlated to wave energy, consistent with other studies that suggest that shoreline erosion is closely related to wind and wind-wave energy (Cerco et al., 2010; Sanford and Gao, 2018). For the present study, shoreline erosion inputs were converted to the flux of sediments from two distinct mud components, clay and silt, into surface waters (Table 1, Table S2). Sand was assumed to settle out too quickly to contribute to surface water clarity (Davies-Colley and Smith, 2001) and was thus ignored in shoreline erosion inputs. Watershed model clay inputs were split into the two corresponding simulated sediment classes of clay-rich flocs and unaggregated mud (Table 1). Spatially, to convert inputs from the watershed regulatory model segment-sheds, inputs were summed for each separate Maryland and Virginia county. County total inputs were then evenly distributed over the land-adjacent water grid cells in ChesROMS-ECB that most closely corresponded to the geographic location of each county's shoreline. Shoreline erosion sediment inputs were implemented as the flux of sediments into surface water grid cells (Fig. 1).

2.2.3. Ballasting effect for particle sinking rates

A further improvement to ChesROMS-ECB included adding a ballasting effect for particle sinking rates. Organic and inorganic particles are known to ballast one another, increasing overall particle sinking rates (e.g., Malpezzi et al., 2013). This enhanced sinking rate was incorporated here as a simplified process to represent how aggregation enhances particle sinking rates in turbid waters. In past studies, updated parameterizations for particle aggregation and sinking improved the performance of biogeochemical models in the Atlantic and Pacific Oceans (Fischer and Karakaş, 2009; Kriest, 2002; Niemeyer et al., 2019). Considering divergent theories on whether organic particles enhance the sinking rates of mineral particles (Kranck and Milligan, 1980; Passow, 2004), mineral particles enhance the sinking rates of organic matter (Armstrong et al., 2001; Klaas and Archer, 2002), or both, depending on composition (Hamm, 2002). In the present study both inorganic and organic particles were simultaneously subjected to a ballasting effect. All particle types were formulated to sink at higher velocities, implemented according to the function:

$$\begin{aligned} &When\ TSS > TSS_{max}, W_s = W_{max} \\ &When\ TSS > TSS_{min}, W_s = W_{min} \\ &When\ TSS_{min} < TSS < TSS_{max}, W_s = \frac{(W_{max} - W_{min})}{(TSS_{max} - TSS_{min})} * TSS + W_{min} \end{aligned} \quad (2)$$

where W_s is the settling velocity for a respective particle type (inorganic: sand, silt-rich flocs, clay-rich flocs, and unaggregated mud; organic: phytoplankton, small detritus, and large detritus). W_{max} and W_{min} are the minimum and maximum settling velocities for each given particle type, set here such that $W_{max} = 4*W_{min}$. TSS_{max} and TSS_{min} are the concentrations at which sinking rates for all particle types begin to increase and reach their maxima, respectively. For simplicity, W_s for a given particle class was assumed uniform over the vertical water column at a given horizontal grid point and time-step. Thus, TSS concentrations at surface grid cells were used to determine the degree of ballasting at each location at each time step, with TSS_{max} and TSS_{min}, respectively, set to 18 and 100 mg L^{-1} (Fig. S3). Conditions with near-surface TSS > 18 mg L^{-1} are mostly encountered in the estuarine turbidity maximum (ETM), defined spatially for the Chesapeake Bay as the region from ~39.1°N to 39.4 °N latitude (Fig. 1). The addition of this ballasting effect mimics the comparatively higher particle settling rates observed in the ETM compared with the mid- and lower-Bay (Sanford et al., 2001).

A run was also conducted in which the ballasting effect was removed, so that sinking rates did not increase in regions of high surface water TSS concentrations. The results were compared to an analogous run with ballasting (Table S3), demonstrating that the ballasting effect improved model skill. Particularly, improvements were found in the surface waters of the upper-Bay ETM, where long-term average modeled FSS and TSS were previously overestimated compared to observed values before the ballasting effect was incorporated. As a result, the ballasting effect was implemented in all model experiments.

2.2.4. Calculation of K_d, Z_{SD}, and TSS

For implementation in ChesROMS-ECB, equations for K_d and Z_{SD} were derived from multiple linear regression analysis using CBP Water Quality Database observations (EPA, 2012) from 1998 to 2019 (see Section 2.1). Modeled K_d was calculated as a function of modeled TSS and salinity, as is common in other Chesapeake Bay modeling studies (Cerco and Noel, 2017; Feng et al., 2015; Xu et al., 2005). Here, updated empirical constants were derived from multiple linear regression analysis (Fig. S4) to incorporate more recent observations with reliable TSS (mg L^{-1}) measurements from January 1998 to December 2019:

$$K_d = 0.92 + 0.079*\mathrm{TSS} - 0.037*Salinity \quad (3)$$

with salinity considered as a proxy for colored dissolved organic matter (and possibly other indirect factors such as nutrient concentrations, which are also inversely correlated with salinity). Eq. (3) is used throughout the model domain and represents a best fit to the data collected throughout the Bay's mainstem. In addition, K_d was bounded by a minimum of 0.04 m^{-1} to represent the attenuation of pure water (Fasham et al., 1990; Fennel et al., 2006). Using the same procedure, modeled Z_{SD} was calculated as a function of modeled K_d and VSS based on CBP data from 1998 to 2019 (Fig. S4):

$$Z_{SD} = \frac{1.46}{(K_d + 0.12*VSS)} \quad (4)$$

Attempts to include additional variables such as particulate carbon or chlorophyll did not improve the empirical relationship for K_d or Z_{SD}. Note that Z_{SD} was only calculated diagnostically from the model output and did not affect the biogeochemical variables, because PAR and K_d are more appropriate measures of light for calculating primary production. Thus, Z_{SD} was used only for post-processing, including model-data comparison and analysis of results.

Modeled TSS was calculated from the concentrations of modeled state variables, using a set of assumptions about the nature of the suspended materials in the Chesapeake Bay based on observed relationships. TSS is the sum of dry weight (DW) concentrations of fixed suspended solids (FSS) and VSS in mg L^{-1}, and VSS is defined to be proportional to particulate organic carbon (POC) concentration:

$$VSS = 2.9*POC \quad (5)$$

where 2.9 is a typical DW VSS:POC ratio for Chesapeake Bay waters (Cerco and Noel, 2017). Modeled POC was calculated as the sum of planktonic and detrital carbon concentrations, where phytoplankton and zooplankton state variables were converted from nitrogen to carbon units using the Redfield ratio. Modeled FSS was computed as the sum of water column inorganic suspended solids (ISS) concentrations from the sediment model (i.e., the sum of silt-rich flocs, clay-rich flocs, and unaggregated mud) and water column VSS multiplied by a constant representing plankton ash content (Fall, 2020):

$$FSS = ISS + 0.35*VSS \quad (6)$$

where 0.35 was the $FSS:DW_{phyto}$ ratio, i.e., the ratio of plankton ash content to plankton total dry weight. This adjustment is required because FSS observations from the CBP Database include ash from plankton-derived solids, but the sediment classes output by the ChesROMS-ECB do not. The 0.35 value in Eq. (6) imitated a representative Chesapeake Bay phytoplankton community made up of 63% diatoms, i.e., a diatom fraction (f_{dia}) of 0.63 (Marshall et al., 2006):

$$FSS:DW_{phyto} = (FSS:DW_{dia}*f_{dia}) + (FSS:DW_{nondia}*(1-f_{dia})) \quad (7)$$

where the ash content to dry weight ratio of diatoms ($FSS:DW_{dia}$) was 0.46 and the ash content to dry weight ratio of non-diatom species ($FSS:DW_{nondia}$) was 0.16 (Whyte, 1987).

2.3. Model simulations and analysis

2.3.1. Reference Run

A realistic Reference Run was conducted over the years 2001–2005. This timeframe encapsulates the high interannual variability of the Chesapeake Bay regional climatic conditions, as it includes two hydrologically dry years (2001−2002), two wet years (2003–2004), and one moderate year (2005). Initial conditions were derived from output of multi-year runs for biogeochemistry and sediment grain size distributions conducted with earlier versions of the modeling framework (Da et al., 2018; Moriarty et al., 2021). Shoreline erosion sediment inputs for the Reference Run were realistic inputs for the early 2000s with a moderately erodible seabed governed by $\tau_{crit(E,D)} = 0.09$ Pa. Additionally, the Reference Run was preceded by one year of model spin-up (2000).

2.3.2. Experiments

In addition to the Reference Run, two experimental runs "More Shoreline Erosion" and "Highly Armored Shoreline Erosion" were conducted to explore how increased shoreline erosion and the absence of shoreline erosion impacted water clarity. For the More Shoreline Erosion run, daily shoreline erosion inputs were doubled, and a concurrent increase in seabed erodibility was implemented ($\tau_{crit(E,D)} = 0.03$ Pa, e.g., Cerco et al., 2013; Moriarty et al., 2021; Cerco et al., 2010). For the Highly Armored Shorelines run, sediment inputs from shoreline erosion were completely removed, and the associated seabed erodibility was decreased ($\tau_{crit(E,D)} = 0.12$ Pa, e.g., Maa et al., 1998; Sanford and Maa, 2001; Wu et al., 2018). The corresponding changes in seabed erodibility for each shoreline change experiment represented the alteration of sediment supply, depositional processes, and grain size distributions commonly observed in response to varying degrees of shoreline armoring (Dugan et al., 2011). Studies addressing interannual variation in estuarine sediment dynamics (Burchard et al., 2018; Dickhudt et al., 2009; Ralston and Geyer, 2009) have demonstrated that shifts in the external supply and internal deposition rates of fine sediment commonly lead to corresponding shifts in bed erodibility.

2.3.3. Analysis of model results

Spatial and temporal patterns in simulated FSS, VSS, TSS, K_d^{-1} and Z_{SD} from each experimental run were compared to those from the Reference Run to assess the spatial extent and seasonal timing of water clarity improvement or degradation according to each metric. Analysis of model results focused on surface waters where phytoplankton production is concentrated, and in the mainstem Bay where incongruous long-term water clarity trends have been observed (Harding et al., 2016). Water clarity differences between the two most contrasting experimental model runs (Highly Armored Shorelines minus More Shoreline Erosion) are described, in order to highlight the spatial and temporal effects of erosional changes. Two "zones" of water clarity change due to the removal of shoreline erosion are defined:

Enhanced Visibility Zone:

Highly Armored minus More Shoreline Erosion, $\Delta K_d^{-1} > 0$ m and $\Delta Z_{SD} > 0$ m

Organic Fog Zone:

Highly Armored minus More Shoreline Erosion, $\Delta Z_{SD} < 0$ m

3. Results

3.1. Model-data comparison

Reference run results were generally consistent with observed physical and clarity-related conditions in surface waters for long-term interannual average conditions for 2001 to 2005 (Table 2). Along the mainstem, long-term mean salinity varied from 0 to 30 with a similar along-Bay distribution in both the model results and observations. Although model results slightly underestimate K_d^{-1} in the lower Bay in 2003, throughout most of the Bay the model reproduces K_d^{-1} and Z_{SD} quite well. Observed long-term mean K_d^{-1} varied from 0.4 to 2 m from the ETM to the Bay mouth, while modeled long-term mean K_d^{-1} varied from 0.3 to 3 m along the same span of locations. Observed long-term mean Z_{SD} ranged down-estuary from 0.4 to 3 m, and modeled Z_{SD} varied between 0.3 and 3 m along the same spatial gradient. At the Bay mouth, slight overestimation of VSS and underestimation of FSS combined to yield a high-skill estimate of TSS and K_d^{-1}. In the ETM, particularly north of 39.4°N latitude (Fig. 1), biases in VSS and FSS resulted in a slight yet consistent overestimation of TSS in all years. Consequences of these biases for light penetration in terms of K_d^{-1} were minimal, since the combination of slight overestimations for both TSS (~1.4 mg L^{-1} higher than observed) and salinity (~0.9 psu higher than observed) balanced one another to effectively represent K_d^{-1} with high skill based on the empirical equation used.

Interannual variability in modeled water clarity conditions closely resembled observed interannual variability between dry and wet years (Fig. 2, Table S4). For example, K_d^{-1} in dry years ranged between 0.7 and 5 m in observations vs. 0.6 and 4 m in the model, and in wet years ranged from 0.5 to 3 m in observations vs. 0.5 to 2 m in the model. Similarly, Z_{SD} in dry years varied from 0.8 to 3 m in observations vs. from 0.5 to 3 m in the model, and in wet years ranged between 0.4 and 2 m in observations vs. 0.3 and 2 m in the model. In dry years, the model slightly underestimated K_d^{-1} and Z_{SD} (i.e., shallower than observed) in the ETM (Fig. 2). There were also larger water clarity differences between wet and dry years in modeled TSS. Observed annual mean TSS was ~1.3 mg L^{-1} greater in wet years than dry years, while modeled TSS was ~4 mg L^{-1} greater in wet years (Table S4). This wet-year-to-dry-year difference was greater in the model due to a combination of VSS and FSS overestimation in wet years.

Model results also successfully reproduced seasonal variability in observed conditions (Fig. S5). Observed K_d^{-1} and Z_{SD} were shallower in May to August compared with February to April, and the model effectively reproduced this seasonal pattern. Modeled Z_{SD} was slightly shallower than observed Z_{SD}, especially in February to April. This shallow Z_{SD} bias of the model reflects a combination of the biases in both K_d^{-1} and VSS during the same season.

Table 2
Reference run model-data comparison for surface water variables over the timeframe January 1, 2001 to December 31, 2005 for the 33 stations in the mainstem Chesapeake Bay.

Variable	$Mean_{modeled}$	$Mean_{observed}$	Bias[a]	N_{obs}
Salinity	14.96	14.06	0.90	2408
K_d^{-1} (m)	1.28	1.72	−0.45	1967
Z_{SD} (m)	1.23	1.46	−0.24	2388
FSS (mg L^{-1})	5.92	4.84	1.08	1387
VSS (mg L^{-1})	3.53	3.16	0.38	982
TSS (mg L^{-1})	9.45	8.08	1.38	2401
Temperature (°C)	15.93	17.26	−1.33	2408

[a] Bias is calculated as $Mean_{modeled}$ - $Mean_{observed}$.

3.2. Spatial variability in the effect of decreased shoreline erosion

Based on the differences between the results of the two contrasting experiments (Highly Armored Shorelines minus More Shoreline Erosion), the removal of shoreline erosion increased light penetration to depth according to K_d^{-1}, but had complex effects on Z_{SD}. In many regions of the Bay, such as shallow, nearshore areas and the upper Bay ETM, the removal of shoreline erosion improved clarity in terms of all metrics in February to April (Fig. 3). However, a complex water clarity effect was observed during that same season in mid-Bay main channel waters: water clarity was improved in terms of decreased FSS and deeper K_d^{-1} while also showing increased VSS and shallower Z_{SD} (Fig. 3). In short, water clarity in terms of light penetration improved, while water transparency declined due to the increased organic matter concentration.

The spatial pattern of clarity change due to the removal of shoreline erosion can be summarized by defining spatial "zones" of change. These water clarity effect zones describe the spatial regions where surface waters showed contrasting impacts of removing shoreline erosion (Fig. 4). In the Enhanced Visibility Zone, reduced sediment inputs improved water clarity in terms of all metrics. This zone represents the portions of the Bay where surface TSS concentrations were sufficiently high in the More Shoreline Erosion model run that TSS reduction improved clarity, but not to the point that enhanced organic matter production overwhelmed the effect of lower TSS on Z_{SD}. In the Organic Fog Zone, reduced sediment inputs improved water clarity in terms of K_d^{-1} (Fig. 4a), yet degraded water clarity in terms of Z_{SD} (Fig. 4b). The Organic Fog Zone occurred in the central channel of the Bay, reaching its maximum extent from station CB4.2C in the northern mid-Bay (~38.65°N) parallel to the Choptank River mouth, down to station CB5.5 in the southern mid-Bay (~37.69°N) just northeast of the Rappahannock River (Fig. 4c). In this zone, concentrations of TSS were such that further sediment reduction deepened K_d^{-1} enough to strongly enhance phytoplankton growth, increasing the organic matter present in surface waters to such a degree that it reduced overall water transparency. The spatial extent of the Organic Fog Zone accounted for up to 20% of the total surface area of the mainstem Chesapeake Bay (Fig. 4c).

The overall effects of the removal of shoreline erosion on water clarity were greater in magnitude at the southern end of the mid-Bay than the northern end. For example, at more southern station CB5.5, highly armored shorelines increased (deepened) K_d^{-1} up to 1 m (Fig. 5). Although the More Shoreline Erosion model run resulted in similar conditions at both the northern and southern mid-Bay stations, the Highly Armored Shoreline run yielded deeper K_d^{-1} and Z_{SD} more so at the southern station (Fig. 5d-f) than at the northern station (Fig. 5a-c). This north-south difference likely reflects the distance from riverine sediment inputs. For example, where riverine sediment inputs still make up a significant contribution to TSS in the upper Bay, removing shoreline erosion yielded only slightly deeper K_d^{-1} and Z_{SD} (Fig. 5a, b), but farther down-estuary the removal of shoreline erosion yielded much deeper K_d^{-1} and Z_{SD} (Fig. 5d, e), not because erosion was greater there, but rather because the relative influence of riverine sediments was lower. This spatial difference in clarity improvement was especially

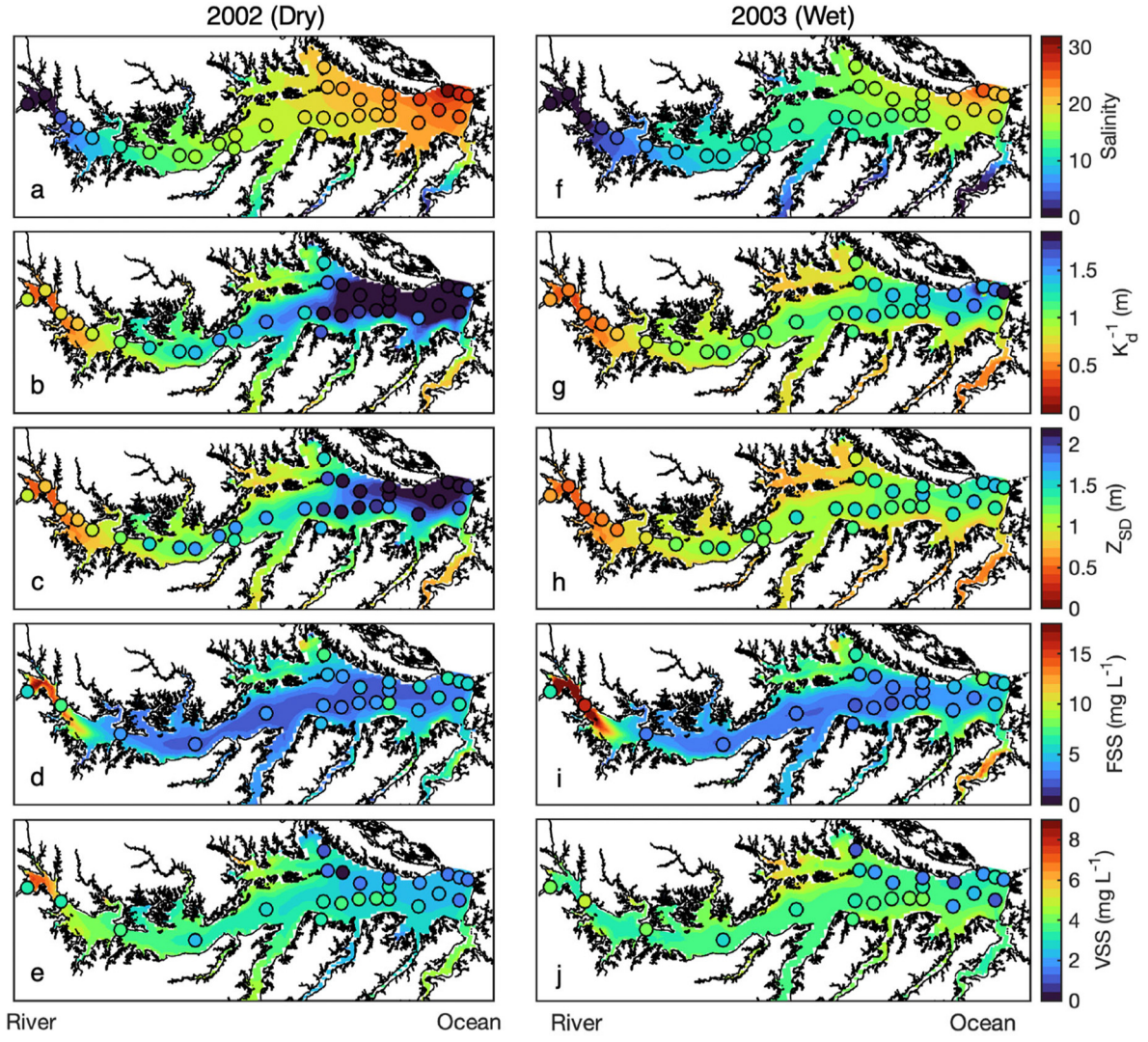

Fig. 2. Reference run model-data comparison for mean **a-e** dry year 2002 conditions and **f-j** wet year 2003 conditions, including variables **a, f** salinity, **b, g** attenuation depth (K_d^{-1}), **c, h** Secchi depth (Z_{SD}), **d, i** fixed suspended solids (FSS), and **e, j** volatile suspended solids (VSS) in surface waters. Circles indicate long-term averages of CBP monitoring cruise observations in surface waters (<2 m) in the mainstem region of the Bay. (For long-term seasonal differences in model-data comparison, see Fig. S5 in supplementary material).

pronounced in winter (see Section 3.3.1) and in dry years (see Section 3.3.2).

3.3. Temporal variability in the effect of decreased shoreline erosion

3.3.1. Seasonal variability

Differences in water clarity due to the removal of shoreline erosion varied in magnitude and spatial extent based on time of year. For example, October to January showed the largest water clarity improvements in both the southern and northern end of the central bay (Fig. 5), presumably because that is the time of year that wave-driven erosion is strongest relative to riverine sediment input. In contrast, February to April showed the greatest increase in organic matter production due to the removal of shoreline sediment inputs (Fig. 3), because that is when increased river discharge provides nutrients that drive the enhanced late winter to early spring bloom in relatively clearer water. Thus, enhanced visibility in term of both Z_{SD} and K_d^{-1} generally occurred during October to January, and the counterintuitive effect on Z_{SD} vs. K_d^{-1} in surface waters had the largest spatial extent during February to April (Fig. 4). The seasonal difference in effects was most clearly visible at the southern mid-Bay station for K_d^{-1} (Fig. 5d). Seasonal patterns in the occurrence of the Organic Fog Zone generally followed seasonal patterns in organic matter concentration.

3.3.2. Interannual variability

Changes in water clarity due to shoreline erosion varied interannually, due to factors that varied between hydrologically wet and dry years (e.g., riverine nutrient and sediment loading); these wet-dry year differences also varied by location down-estuary (Fig. 5). In all model experiments, K_d^{-1} and Z_{SD} were both deeper in dry years (2001 and 2002) than wet years (2003 and 2004). However, the difference between wet years and dry years was most pronounced for the Highly Armored Shorelines run for K_d^{-1} at station CB5.5 (Fig. 5d) than at station CB4.2C (Fig. 5a). Conversely, the difference between wet years and dry years was less pronounced for the More Shoreline Erosion run. The timing of the occurrence of the Organic Fog Zone was slightly different each year and with distance down-estuary. For example, in dry years of 2001 and 2002, the northern mid-Bay station showed an Organic Fog Zone as early as January (Fig. 5c). Also, an Organic Fog Zone only occurred in the fall season during wet year 2003. The spatial extent of the Organic Fog Zone also varied between dry and wet years. In dry years, Organic Fog Zone effects occurred more often at the northern station (CB4.2C; Fig. 5c) than the southern station (CB5.5; Fig. 5f); however, in wet years, Organic Fog Zone conditions were more common in the southern mid-Bay than in the northern mid-Bay.

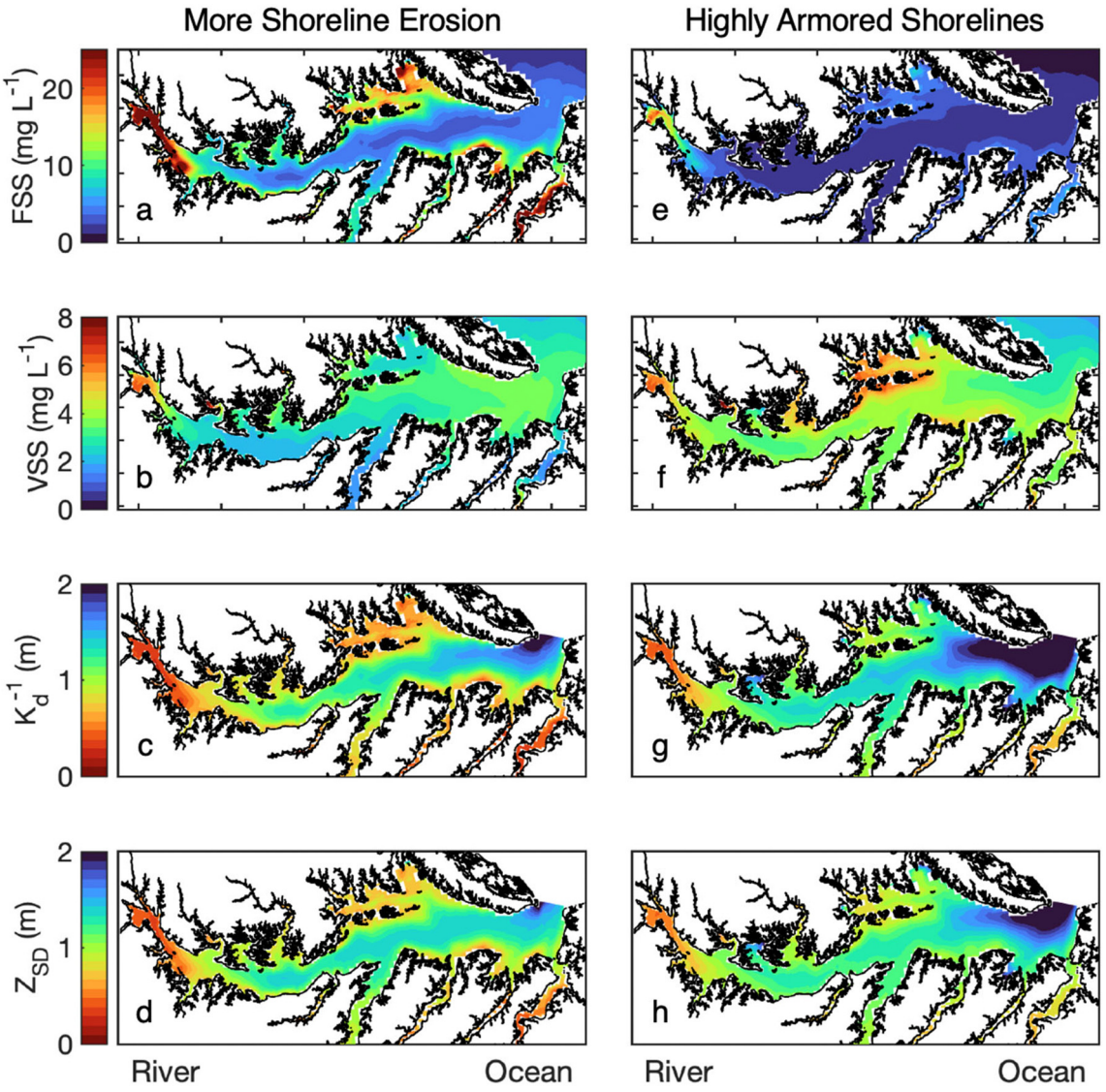

Fig. 3. February to April 2001 results of **a-d** More Shoreline Erosion run, **e-h** Highly Armored Shorelines run for **a, e** fixed suspended solids (FSS), **b, f** volatile suspended solids (VSS), **c, g** attenuation depth (K_d^{-1}) and **d, h** Secchi depth (Z_{SD}) in surface waters.

4. Discussion

4.1. Overall impact of coastal erosion on water clarity

Model experiments quantified the direction and magnitude of change in water clarity when coastal erosion alters sediment inputs. Specifically, the experiments showed the variability of impacts on water clarity according to multiple metrics (VSS, FSS, K_d^{-1}, and Z_{SD}), between different locations down-estuary, among different seasons, and among years with different hydrological conditions. Water clarity in terms of light attenuation depth (K_d^{-1}) improved when shoreline erosion sediment inputs were removed. Coastal erosion impacts the lower Bay more than the upper Bay, not necessarily due to spatial differences in erosion, but due to the spatially limited influence of riverine sediments. Thus, erosion has a relatively larger effect with distance from river sources, particularly in dry years (2001–2002). For example, the removal of shoreline erosion has a greater impact farther down-estuary, particularly in dry years (Fig. 4, Fig. 5), likely because under dry hydrological conditions, relatively less riverine sediment contributes to TSS concentrations farther down-estuary. Despite water clarity improvement in terms of illumination (deeper K_d^{-1}), model results indicate that under certain conditions, decreased sediment inputs to the mainstem of the estuary can contribute to shallower Z_{SD} in the mid-Bay (Fig. 6), here defined as the Organic Fog Zone. These opposing impacts on K_d^{-1} and Z_{SD} were seen in certain locations and seasons depending on hydrological conditions. In dry years, Organic Fog Zone effects occurred more often at its northern than southern extent; however, in wet years, Organic Fog Zone conditions were more common farther south (Fig. 5). Most likely, increased riverine nutrients supported organic matter production in wet years farther down-estuary than in dry years. Additionally, it may be that greater light limitation in wet years compared to dry years in the mid- to upper-Bay (northern station in Fig. 5) allowed nutrients to remain available down-estuary in wet years to fuel organic production and create an Organic Fog Zone effect farther south. Even though the occurrence of the Organic Fog Zone is a seasonal and somewhat sporadic phenomenon, it has important implications.

4.2. Implications of water clarity change for bio-optics

The patterns in water clarity change due to shoreline armoring are relevant to previous bio-optical theories stating that opposite long-term trends in Z_{SD} and K_d^{-1} are caused by increased light scattering via changing particle composition. Gallegos et al. (2011) hypothesized

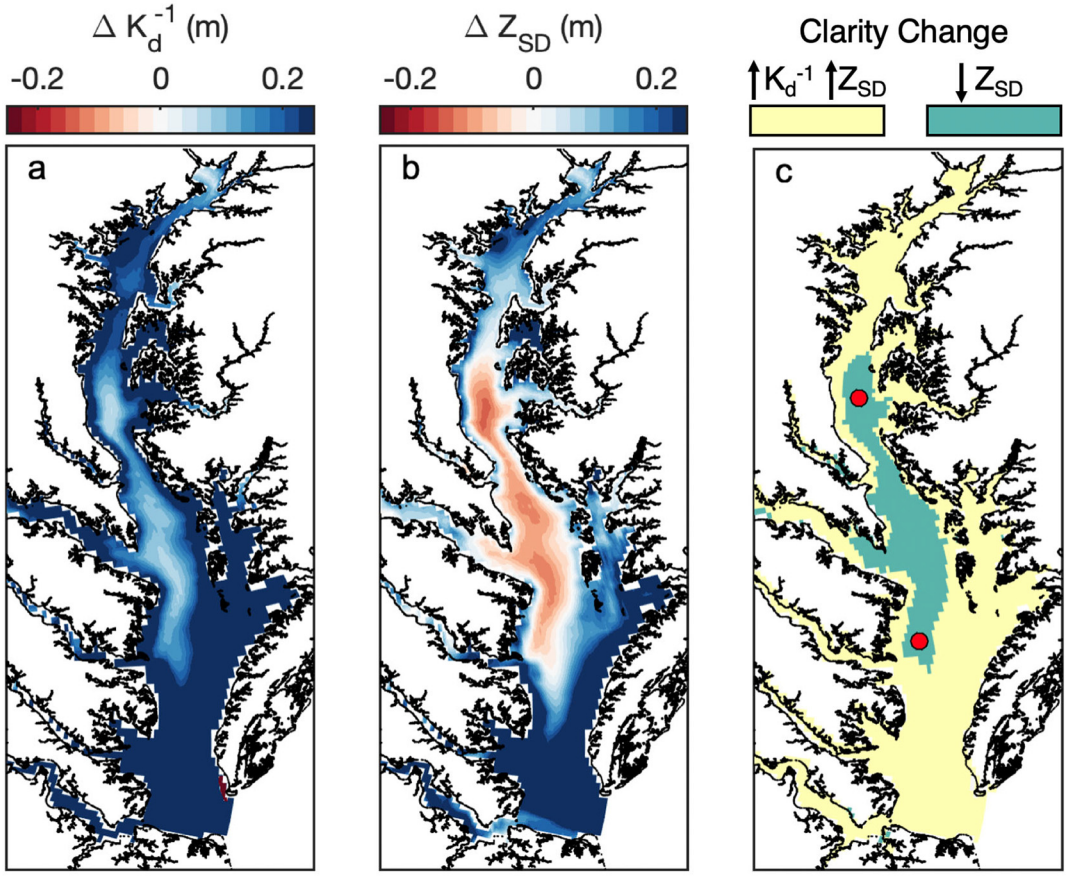

Fig. 4. Changes due to reduced shoreline erosion February to April 2001, including **a** K_d^{-1} effects and **b** Z_{SD} effects in surface waters, in terms of the difference (Δ) between Highly Armored Shorelines minus More Shoreline Erosion. Blue colour in difference plots represents clearer water in terms of each metric. Zones **c** of clarity change are defined by the respective ΔK_d^{-1} and ΔZ_{SD} shown in **a** and **b**. Zones in **c** are defined as: Enhanced Visibility Zone (yellow) with $\Delta K_d^{-1} > 0$ m (deeper) and $\Delta Z_{SD} > 0$ m (deeper); Organic Fog Zone (green) with $\Delta Z_{SD} < 0$ m (shallower). Colour scales in left two subplots were selected to highlight the central channel or mainstem of the Bay: in subplot **a**, ΔKd^{-1} ranged from 0.01 to 0.8 m; In subplot **b**, ΔZ_{SD} ranged from −0.14 to 0.7 m. Circles in **c** indicate stations CB4.2C and CB5.5, highlighting the northern and southern extents of the organic fog zone (see Fig. 5).

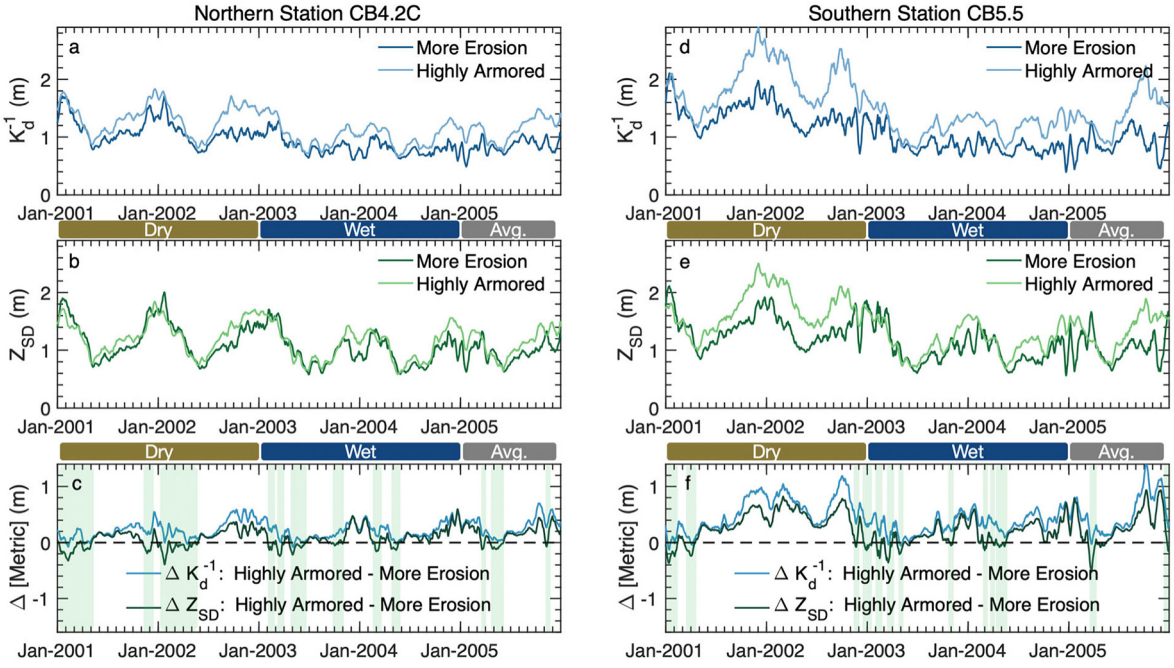

Fig. 5. Time series of surface water effects at the typical **a-c** northern extent and **d-f** southern extent of the organic fog zone, including **a, d** K_d^{-1}, **b, e** Z_{SD}, and **c, f** differences in both clarity metrics due to the removal of shoreline erosion, in terms of Highly Armored Shorelines minus More Shoreline Erosion. Green shading in bottom panels indicates the occurrence of an organic fog zone, i.e., with $\Delta Z_{SD} < 0$ m. Lines were smoothed with a 15-day moving average. See Fig. 4 for station locations.

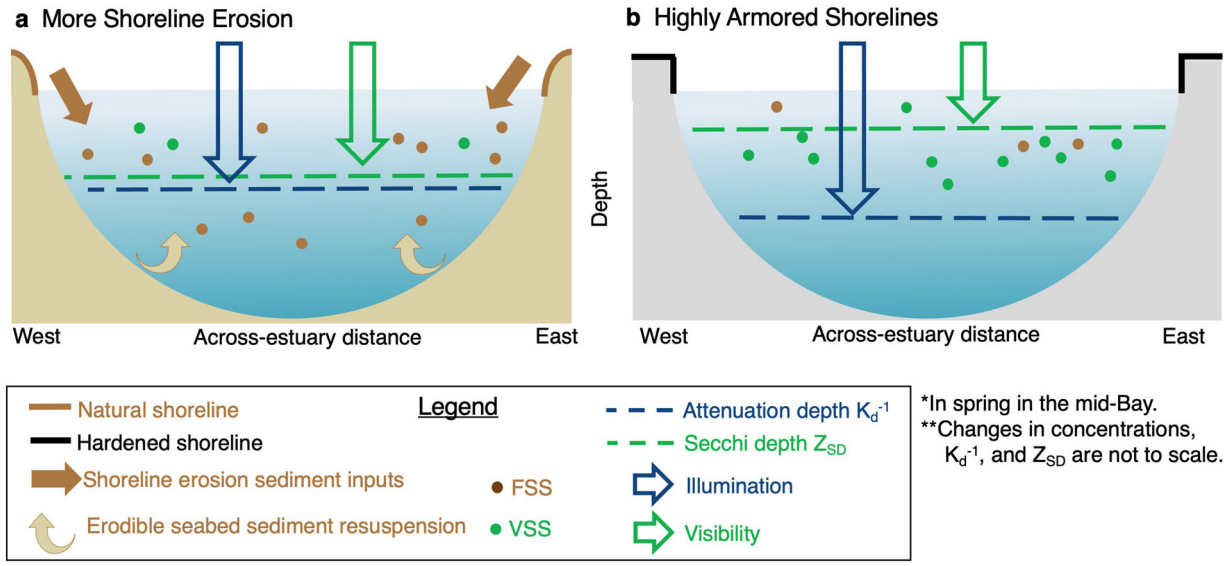

Fig. 6. Conceptual diagram of water clarity changes in an idealized across-estuary transect through the mid-Bay during times of high organic solids concentrations (February–April), in model runs **a** More Shoreline Erosion and **b** the Highly Armored Shorelines. Changes shown are particular to the Organic Fog Zone region in deep waters. Relative concentrations and clarity depths are not drawn to scale.

that shallowing Z_{SD} despite deepening K_d^{-1} over time was due to an increase in small organic detrital particles caused by their light scattering behavior. Results of model experiments in this study supported that organic detritus hypothesis. In mainstem, mid-Bay waters, at sufficient distance from riverine influence, organic particle concentrations increased when shoreline erosion was removed (Fig. 3), often causing opposite effects on K_d^{-1} and Z_{SD} (Fig. 4). Reduced sediment inputs to the mid- and lower-Bay could thus help explain an increased organic-to-inorganic ratio for suspended solids, particularly when more organic matter is produced due to relaxed light limitation. Spatially, the mid-Bay is categorized as a "hypertrophic" estuarine environment due to its extremely high production of organic matter (Harding et al., 2020); thus, the small organic detritus hypothesis may apply specifically to changes in scattering behavior of particles in the mid-Bay where an Organic Fog Zone often occurs. This study thus identifies a mechanism for changing light-scattering behavior of particles in the lower-TSS, hypertrophic, highly productive regions of the Bay.

4.3. Relevance to long-term trends, restoration, and management

To put the results of the present study into management context, it is important to consider the role of shoreline erosion among other mechanisms of water clarity change. First, the somewhat small magnitudes of opposing clarity effects, on average ~10 cm shallower Z_{SD} with ~10 cm deeper K_d^{-1} (Fig. 3, Fig. 4) suggest that shoreline armoring over time may only partially explain observed incongruous long-term changes in K_d^{-1} and Z_{SD}. For example, previous studies have shown that Z_{SD} in the mainstem has shallowed more than 10 cm since 1985 (Keisman et al., 2019; Murphy et al., 2019; Testa et al., 2019; Williams et al., 2010). In addition, a simple linear regression using the 33 mainstem stations in the present study shows that Z_{SD} has shallowed approximately 29 cm from 1985 to 2019. Degraded water transparency despite increased light availability is likely an even more complex trend than what has been described in the present study. For example, sensitivity testing revealed that the removal of shoreline erosion alone, with no resulting change in seabed erodibility in terms of critical shear stress, only elicited ~2 cm shallower Z_{SD}. This suggests that the relationship between sediment inputs and seabed erodibility is a crucial driver of water clarity (see Section 4.5).

In a heavily-managed region, the applicability of the two water clarity metrics (Z_{SD} vs. K_d^{-1}) should be considered for different purposes. The results of the model experiments in this study clearly indicate that these two metrics respond differently to reductions in sediment inputs (Fig. 4). Thus, they should be applied independently depending on the study goals. For example, K_d^{-1} as a measurement is most useful for applications that study autotrophs, including submerged aquatic vegetation, water column phytoplankton, and benthic microalgae (Mangan et al., 2020). On the other hand, Z_{SD} is more relevant for applications whose goal is to measure transparency and visibility. Applications for Z_{SD} may include recreational fishing, fish predation on lower trophic levels (Benfield and Minello, 1996), relative abundance of predatory fish vs. mesopredators (Reustle and Smee, 2020), and waterfront property values (Klemick et al., 2018; Moore et al., 2020; Walsh et al., 2017).

In light of ongoing restoration projects that depend on water clarity, such as submerged aquatic vegetation beds and oyster reefs, it is similarly crucial to consider the metrics K_d^{-1} and Z_{SD} independently. As seen in the results of this study, the two metrics can have opposite directions of change based on a shift in the composition of suspended solids in surface waters (Fig. 4). In other water bodies experiencing oligotrophication, the incongruity of Z_{SD} and K_d^{-1} has different implications from what is occurring in Chesapeake Bay, providing additional reasons to separate trends in the different metrics. In a Danish fjord (Pedersen et al., 2014), Z_{SD} deepened over time more quickly than might be predicted based on a linear relationship with K_d^{-1} as suspended particulate matter decreased. K_d^{-1} remained somewhat high because of dissolved light-absorbing constituents despite improved transparency. For this fjord with increasing visibility, Z_{SD} overestimated the depths of potential seagrass habitat (Pedersen et al., 2014). In the Chesapeake Bay, the results of the current study suggest that using Z_{SD} as the dominant water clarity metric will result in an underestimation of potential seagrass habitat, because an improvement in Z_{SD} often did not consistently co-occur with an improvement in K_d^{-1} (Fig. 6). A constant inverse relationship between Z_{SD} and K_d (e.g., Wang et al., 2013) may be inappropriate for estuarine applications, and the inherent measurement differences could influence the success or failure of restoration projects.

Lastly, sediment loading processes are highly complex, and measures to reduce sediment loading can have secondary consequences to downstream ecosystems. Many management efforts target riverine sediment loads alone; however, these are typically only one of three main sources of inorganic suspended solids. Sediment sources also include shoreline erosion and seabed resuspension. The results of this study indicate that sediment inputs from shoreline erosion are particularly influential in fall and winter seasons when riverine inputs are relatively

low (Fig. 5). Results similarly highlight that where riverine sediment inputs are low in the mid- and lower-Bay, especially in dry years, shoreline erosion and resuspension are major drivers of clarity. It is useful to consider these multiple processes through which sediments affect water clarity, and to consider that manipulation of any one of those processes could have secondary consequences for the ecosystem. Sediment reduction is a frequent goal of watershed management, but according to the present study, reduced sediment inputs do not always improve all measures of water clarity as one might expect.

4.4. Relevance to other coastal systems

Results of this study apply to many other coastal systems worldwide that are similarly characterized by human-impacted sediment supply and variable light limitation of phytoplankton. Many systems also exhibit down-estuary gradients in primary production and turbidity similar to those observed in the Chesapeake Bay (Cloern, 1987; Cloern et al., 2014). For example, the Delaware Bay (Dijkstra et al., 2019; McSweeney et al., 2017), the Gironde estuary in France (Irigoien and Castel, 1997), and the Westerschelde estuary in the Netherlands (Kromkamp et al., 1995) also experience light-limited primary production which varies in magnitude due to human impacts on nutrient and sediment inputs. In these systems, we would expect response to altered sediment inputs to vary with distance from major river sources, like in the results of this study (Fig. 5). Syntheses have found that, like in the present study, changes in coastal water transparency worldwide in terms of Z_{SD} are indirect responses to eutrophication or oligotrophication (Cloern, 2001). Similar to trends in the Baltic Sea, effects of changing nutrient and sediment supply are spatially heterogeneous in the Chesapeake Bay because of processes specific to the bathymetry, bottom type, vegetation, distance from inputs (Fig. 5), and shoreline type at local scales. Lastly, as we have seen from in our results from the Chesapeake Bay, water clarity improvements will ultimately be somewhat limited by physical sediment transport processes. Sediment resuspension via tides and wind-driven waves often limits water clarity in the Chesapeake Bay, as in the North Sea, the Westerschelde estuary, and some fjords (Olesen, 1996). For example, even in the realistic scenario conducted here, inorganic suspended sediment concentrations were still moderately high ~10 mg L^{-1} in the lower-Bay, especially in the shallower regions east and west of the main channel, due to wind- and tide-driven resuspension (Fig. 2d, i).

Impacts of shoreline armoring in the Chesapeake Bay relate to other human impacts on coastal sediment supply. River impoundments may have similar secondary consequences to those of shoreline armoring for estuaries in the long term. In the results of this study, reduced sediment inputs from shoreline erosion resulted in greater organic matter production due to relaxed light limitation (Fig. 3). In estuaries whose watersheds are heavily dammed, reduced sediment inputs to downstream waters over time can similarly increase the euphotic zone of the estuary and cause long-term increases in primary production. For example, due to dam construction in its watershed, the San Francisco Bay experienced a 50% reduction in turbidity since 1975 (Cloern and Jassby, 2012). Before the construction of structures such as dams and hardened shorelines, management entities should consider what an increased euphotic zone might mean for downstream water bodies, as the altered sediment inputs may have secondary consequences for aquatic ecosystems.

4.5. Recommendations for future work

Although this work incorporated many processes, uncertainties remain that should be taken into consideration for future modeling studies of water clarity. One avenue for future investigation is the plankton ash content of material from in situ suspended solids data used for model calibration and evaluation. In the modeling framework used here, VSS is an estimation of organic matter dry weight including plankton and detritus, and FSS is a simplified estimation of inorganic sediment particles plus the plankton ash content. Because the Chesapeake Bay phytoplankton community composition varies widely in proportions of diatoms vs. other species with different ash contents, the organic-to-inorganic ratio of phytoplankton and associated detritus in our single-phytoplankton-class model was simplified. In terms of model skill, VSS overestimation by the model compared to observations both in the annual average (Table 2) and seasonally in May to August (Fig. S5) may have been partially due to phytoplankton simplification into one class, when in fact there is a seasonal progression of the phytoplankton species composition and corresponding plankton ash content.

Moreover, future work should consider additional processes that impact water clarity, including biogeochemical processes, more detailed optical processes, local sources of runoff, and alternative shoreline stabilization techniques. For example, feedbacks on temperature-driven stratification associated with higher absorption of solar radiation in more turbid waters (Kim et al., 2020), more detailed flocculation of small particles into larger particles (Tarpley et al., 2019), organic content and fractal behavior of flocs (Fall et al., 2021), and more comprehensive nutrient fluxes at the sediment-water interface (Moriarty et al., 2021) could be investigated. Furthermore, although K_d^{-1} demonstrates high model skill (Table 2, Fig. 2), the empirical K_d equation used here was limited by the variables available in the CBP in situ dataset. Therefore, future work could incorporate a K_d formulation based on inherent optical properties, including the spectral contributions of dissolved substances (e.g., Clark et al., 2020), phytoplankton, inorganic sediments, and organic detritus to absorption and scattering. Another limitation of this study is that runoff containing sediment was only introduced at the riverine headwaters (Fig. 1). It is possible that local runoff of sediment and nutrients from the lower coastal plain, which were combined with headwater inputs in this study, may also affect local mainstem water clarity (Williams et al., 2010). Lastly, the effects of multiple shoreline alteration types on estuarine water clarity should be studied. Living shorelines are proposed as an alternative measure to stabilize coastlines while still allowing for some physical and biological connectivity (Bilkovic et al., 2016), yet estuary-scale water clarity impacts of living shorelines vs. traditional shoreline hardening practices remain unknown.

Finally, future work should consider other potential mechanisms for incongruous changes in Secchi depth and light attenuation depth. Counterintuitive water clarity change (Fig. 6) may stem from a shift in phytoplankton community composition and a concurrent change in the optical properties of the living cells and detrital material associated with different species. Related to phytoplankton communities, some research has shown that light limitation increases the likelihood of explosive phytoplankton growth upon greater light availability, creating a negative feedback loop on planktonic health (Buchanan, 2020). This boom-and-bust pattern for light-limited estuarine plankton should be considered in future studies of changing light availability. Future models might also implement a dynamic link between decreased sediment loading and decreased seabed erodibility, i.e., an explicit link between bed erodibility and local sediment supply (Sanford, 2008) as these processes are likely driving water clarity change in a complex way. In the results of this study, distance from riverine inputs impacted the relative effect of shoreline erosion on clarity, yet riverine inputs were kept the same in all model runs for the purpose of specifically examining shoreline erosion effects. In terms of potential riverine impacts, changes in inorganic particle size distributions from riverine sources and shifts in the timing of inputs due to dam infilling (Palinkas and Russ, 2019; Russ and Palinkas, 2020) could alter the clarity-related behavior of suspended particles.

5. Conclusions

Using model experiments, this study investigated the estuary-wide impacts of shoreline armoring on water clarity in terms of suspended

particle composition and two metrics of water clarity: attenuation depth and Secchi depth. In addition to shoreline erosion, the modeling framework included realistic atmospheric forcing, physical processes, biogeochemical cycling, riverine inputs, and resuspension of seabed sediments. In situ cruise-based observations were used to evaluate model results. Our experiments showed that compared to conditions with high shoreline erosion, a Chesapeake Bay estuary with highly armored shorelines and associated reductions in bed erodibility would have widespread increased water clarity in terms of deeper K_d^{-1}. The strongest clarity improvement occurred in the mid- to lower-Bay in dry years, i.e., at locations and times with lower influence of riverine sediment inputs. Yet, under certain conditions, highly armored shorelines resulted in shallower Z_{SD}, especially during seasons and years with high organic matter production. Spatially, the region characterized by shallower Z_{SD} and deeper K_d^{-1} was defined as the Organic Fog Zone. The extent of this Organic Fog Zone varied by season and year, depending on the timing and magnitude of nutrient inputs and organic production. In short, with decreased shoreline erosion sediment inputs, consequences on water clarity were sometimes counterintuitive due to organic matter processes in the estuary. Considering climate change and management efforts in context of the next century, impacts on water clarity may continue to be metric-dependent in the Chesapeake Bay. Questions for the future include: will the Organic Fog Zone expand spatially with future reductions in sediment inputs? Will a climate-driven shift in phytoplankton community composition affect Z_{SD} and K_d^{-1} differently in a warmer Chesapeake Bay? Will changes in storm intensity and wind patterns further alter the resuspension of seabed sediments and influence water clarity? In the long-term, sufficient nutrient reductions may concurrently increase both water transparency and light penetration for unambiguously clearer waters and improved ecosystem health.

CRediT authorship contribution statement

Jessica S. Turner: Data curation, Methodology, Validation, Visualization, Investigation, Writing – original draft. **Pierre St-Laurent:** Software, Data curation, Methodology, Writing – review & editing. **Marjorie A.M. Friedrichs:** Investigation, Methodology, Validation, Supervision, Resources, Writing – review & editing, Funding acquisition. **Carl T. Friedrichs:** Conceptualization, Methodology, Writing – review & editing, Funding acquisition.

Declaration of competing interest

The authors declare that they have no known competing financial interests or personal relationships that could have appeared to influence the work reported in this paper.

Acknowledgments

Many thanks to Julia Moriarty and Courtney Harris for guidance in model development for sediment and seabed parameterizations, including initial seabed grain size conditions. The authors thank Larry Sanford for advice on timing of shoreline erosion sediment inputs and Fei Da and Kyle Hinson for their help with the ECB model. Larry Sanford, Grace Massey, Ken Moore, and Courtney Harris contributed advice and helped with early stages of this project. The authors thank the Virginia Institute of Marine Science Shoreline Studies Program and Center for Coastal Resources Management (CCRM) for curating the shoreline and tidal marsh inventory database (https://www.vims.edu/ccrm/research/inventory/index.php). The authors thank researchers at the Chesapeake Bay Program (CBP) for long-term water quality data (https://datahub.chesapeakebay.net/). We thank Gopal Bhatt at the CBP for sharing the daily-allocated shoreline erosion sediment inputs and other model forcing files from the Chesapeake Bay Watershed regulatory model. Model results are freely accessible and can be downloaded from the William & Mary ScholarWorks data repository corresponding to this article (https://doi.org/10.25773/rh56-4g63). This work used High-Performance Computing facilities at William & Mary, which are supported by the National Science Foundation, the Commonwealth of Virginia Equipment Trust Fund, and the Office of Naval Research. Jay Kanukurthy and Eric Walter provided additional computational support. J. Turner was supported in part by National Science Foundation Grant OCE-1459708 and the Commonwealth Coastal Research Fellowship from the Commonwealth of Virginia. Additionally, this paper is the result of research funded by the National Oceanic and Atmospheric Administration's National Centers for Coastal Ocean Science under award NA16NOS4780207 to the Virginia Institute of Marine Science. We thank 2 anonymous reviewers for their time. This is Virginia Institute of Marine Science contribution number 3984.

Appendix A. Notation

CBP	Chesapeake Bay Program.
ChesROMS-ECB	Chesapeake Bay ROMS Estuarine Carbon and Biogeochemical model.
ERA5	ECMWF *Re*-Analysis, a climate reanalysis product generated by the European Centre for Medium-Range Weather Forecasts (ECMRW).
ETM	Estuarine turbidity maximum, the location near the head of the estuary in low salinity waters characterized by consistently high TSS concentrations. Defined spatially for Chesapeake Bay as waters from ~39.1°N to 39.4 °N latitude.
FSS	Fixed suspended solids concentration (mg L^{-1}), including ISS plus the mass fraction of organic suspended solids remaining on a filter after combustion, i.e., plankton ash content.
ISS	Inorganic suspended solids concentration (mg L^{-1}), synonymous with mineral suspended solids (MSS) concentration.
K_d	Diffuse attenuation coefficient of photosynthetically active radiation (m^{-1}).
K_d^{-1}	Attenuation depth, synonymous with optical depth or light attenuation depth.
Mainstem	Primary downstream segment of the Chesapeake Bay, including the central thalweg or transect of the Bay running from north to south and other surrounding non-tributary waters south of ~39.1°N latitude.
PAR	Photosynthetically active radiation.
ROMS	Regional Ocean Modeling System.
Shoreline erosion	Physical weathering of sediments from banks, cliff, beach, or marshes into adjacent waters. Synonymous with shore erosion and/or coastal erosion.
SWAN	Simulating WAves Nearshore model.
TSS	Total suspended solids concentration (mg L^{-1}), comparable to suspended particulate matter (SPM) or total suspended matter (TSM).
VSS	Volatile suspended solids concentration (mg L^{-1}), the components of organic solids which are volatilized during filter combustion at 550 °C, calculated using the relation TSS = VSS + FSS. Used as a proxy for particulate organic matter (POM).
W_s	Vertical settling velocity of particles (mm s^{-1}).
z	Depth (m).
Z_{SD}	Secchi disk depth (m). Used in the context of transparency and visibility.
$\tau_{crit(ED)}$	Critical shear stress for seabed sediment erosion (E) and deposition (D) (Pa).

Appendix B. Supplementary data

Supplementary data to this article can be found online at https://doi.org/10.1016/j.scitotenv.2021.145157.

References

Armengol, J., Caputo, L., Comerma, M., Feijoó, C., García, J.C., Marcé, R., Navarro, E., Ordoñez, J., 2003. Sau reservoir's light climate: relationships between Secchi depth and light extinction coefficient. Limnetica 22, 195–210.

Armstrong, R.A., Lee, C., Hedges, J.I., Honjo, S., Wakeham, S.G., 2001. A new, mechanistic model for organic carbon fluxes in the ocean based on the quantitative association of POC with ballast minerals. Deep Sea Res. Part II Top. Stud. Oceanogr. 49, 219–236. https://doi.org/10.1016/S0967-0645(01)00101-1.

Benfield, M.C., Minello, T.J., 1996. Relative effects of turbidity and light intensity on reactive distance and feeding of an estuarine fish. Environ. Biol. Fish 46, 211–216. https://doi.org/10.1007/BF00005223.

Bilkovic, D.M., Mitchell, M., Mason, P., Duhring, K., 2016. The role of living shorelines as estuarine habitat conservation strategies. Coast. Manag. 44, 161–174. https://doi.org/10.1080/08920753.2016.1160201.
Bilkovic, D.M., Mitchell, M.M., Davis, Jennifer, Herman, J., Andrews, E., King, A., Mason, P., Tahvildari, N., Davis, Jana, Dixon, R.L., 2019. Defining boat wake impacts on shoreline stability toward management and policy solutions. Ocean Coast. Manag. https://doi.org/10.1016/j.ocecoaman.2019.104945.
Bonsdorff, E., Blomqvist, E.M., Mattila, J., Norkko, A., 1997. Long-term changes and coastal eutrophication. Examples from the Aland Islands and the Archipelago Sea, northern Baltic Sea. Oceanol. Acta 20, 319–329. https://doi.org/10.1016/S0272-7714(97)80008-X.
Booij, N., Ris, R.C., Holthuijsen, L.H., 1999. A third-generation wave model for coastal regions: 1. Model description and validation. J. Geophys. Res. 104, 7649–7666. https://doi.org/10.1029/98JC02622.
Bowers, D.G., Roberts, E.M., Hoguane, A.M., Fall, K.A., Massey, G.M., Friedrichs, C.T., 2020. Secchi disk measurements in turbid water. J. Geophys. Res. Ocean. 125. https://doi.org/10.1029/2020jc016172 e2020JC016172.
Boyer, T.P., Baranova, O.K., Coleman, C., Garcia, H.E., Grodsky, A., Locarnini, R.A., 2018. World Ocean Database 2018. AV Mishonov, Technical Editor. NOAA Atlas NESDIS 87. doi:10.13140/RG.2.2.34758.01602.
Buchanan, C., 2020. A water quality binning method to infer phytoplankton community structure and function. Estuar. Coasts 43, 661–679. https://doi.org/10.1007/s12237-020-00714-3.
Burchard, H., Schuttelaars, H.M., Ralston, D.K., 2018. Sediment trapping in estuaries. Annu. Rev. Mar. Sci. 10, 371–395. https://doi.org/10.1146/annurev-marine-010816-060535.
Cerco, C.F., Noel, M.R., 2017. The 2017 Chesapeake Bay Water Quality and Sediment Transport Model. Vicksburg, MS.
Cerco, C.F., Kim, S.-C., Noel, M.R., 2010. The 2010 Chesapeake Bay Eutrophication Model. A report to the US Environmental Protection Agency Chesapeake Bay Program and to the US Army Engineer Baltimore District.
Cerco, C.F., Kim, S.C., Noel, M.R., 2013. Management modeling of suspended solids in the Chesapeake Bay. USA. Estuar. Coast. Shelf Sci. 116, 87–98. https://doi.org/10.1016/j.ecss.2012.07.009.
Chhor, A.D., Glassman, D.M., Smol, J.P., Vermaire, J.C., Cooke, S.J., 2020. Ecological consequences of shoreline armoring on littoral fish and benthic macroinvertebrate communities in an Eastern Ontario lake. Aquat. Sci. 82. https://doi.org/10.1007/s00027-020-00740-0.
Clark, J.B., Long, W., Hood, R.R., 2020. A comprehensive estuarine dissolved organic carbon budget using an enhanced biogeochemical model. J. Geophys. Res. Biogeosci. 125. https://doi.org/10.1029/2019jg005442 e2019JG005442.
Cloern, J.E., 1987. Turbidity as a control on phytoplankton biomass and productivity in estuaries. Cont. Shelf Res. 7, 1367–1381. https://doi.org/10.1016/0278-4343(87)90042-2.
Cloern, J.E., 2001. Our evolving conceptual model of the coastal eutrophication problem. Mar. Ecol. Prog. Ser. 210, 223–253. https://doi.org/10.3354/meps210223.
Cloern, J.E., Jassby, A.D., 2012. Drivers of change in estuarine-coastal ecosystems: discoveries from four decades of study in San Francisco Bay. Rev. Geophys. 50, 1–33. https://doi.org/10.1029/2012RG000397.
Cloern, J.E., Foster, S.Q., Kleckner, A.E., 2014. Phytoplankton primary production in the world's estuarine-coastal ecosystems. Biogeosciences 11, 2477–2501. https://doi.org/10.5194/bg-11-2477-2014.
Da, F., Friedrichs, M.A.M., St-Laurent, P., 2018. Impacts of atmospheric nitrogen deposition and coastal nitrogen fluxes on oxygen concentrations in Chesapeake Bay. J. Geophys. Res. Ocean. 123, 5004–5025. https://doi.org/10.1029/2018JC014009.
Copernicus Climate Change Service (C3S) (2017): ERA5: Fifth generation of ECMWF atmospheric reanalyses of the global climate. 2017. Copernicus Climate Change Service Climate Data Store. Retrieved from https://cds.climate.copernicus.eu/cdsapp#!/home
Davenport, T., 2012. The Consequences of Shoreline Development for Near-shore Communities in Chesapeake Bay, USA: A Before-after Control-impact Study. doi:10.25773/v5-w538-hx39.
Davies-Colley, R.J., Smith, D.G., 2001. Turbidity, suspended sediment, and water clarity: a review. J. Am. Water Resour. Assoc. 37 (5), 1085–1101. https://doi.org/10.1111/j.1752-1688.2001.tb03624.x.
Dickhudt, P.J., Friedrichs, C.T., Schaffner, L.C., Sanford, L.P., 2009. Spatial and temporal variation in cohesive sediment erodibility in the York River estuary, eastern USA: a biologically influenced equilibrium modified by seasonal deposition. Mar. Geol. 267, 128–140. https://doi.org/10.1016/j.margeo.2009.09.009.
Dijkstra, Y.M., Chant, R.J., Reinfelder, J.R., 2019. Factors controlling seasonal phytoplankton dynamics in the Delaware River Estuary: an idealized model study. Estuar. Coasts https://doi.org/10.1007/s12237-019-00612-3.
Druon, J.N., Mannino, A., Signorini, S., McClain, C., Friedrichs, M., Wilkin, J., Fennel, K., 2010. Modeling the dynamics and export of dissolved organic matter in the Northeastern U.S. continental shelf. Estuar. Coast. Shelf Sci. 88, 488–507. https://doi.org/10.1016/j.ecss.2010.05.010.
Dugan, J.E., Airoldi, L., Chapman, M.G., Walker, S.J., Schlacher, T., 2011. Estuarine and coastal structures: environmental effects, a focus on shore and nearshore structures. Treatise on Estuarine and Coastal Science. 8, pp. 17–41. https://doi.org/10.1016/B978-0-12-374711-2.00802-0.
Easton, Z., Scavia, D., Alexander, R., Band, L., Boomer, K., Kleinman, P., Martin, J., Miller, A., Pizzuto, J., Smith, D., Welty, C., 2017. Scientific and Technical Advisory Committee Chesapeake Bay Watershed Model Phase 6 Review STAC Review Report 47, 1–47. Retrieved from http://scavia.seas.umich.edu/wp-content/uploads/2018/03/Easton-et-al.-2017.pdf
Effler, S.W., Peng, F., 2012. Light-scattering components and Secchi depth implications in Onondaga Lake, New York. USA. Fundam. Appl. Limnol. für Hydrobiol. 179, 251–265. https://doi.org/10.1127/1863-9135/2012/0177.
Effler, S.W., Gelda, R., Perkins, M.G., Peng, F., Hairston, N.G., Kearns, C.M., 2008. Patterns and modeling of the long-term optics record of Onondaga Lake, New York. Fundam. Appl. Limnol. 172, 217–237. https://doi.org/10.1127/1863-9135/2008/0172-0217.
Environmental Protection Agency (EPA), 2012. Guide to Using Chesapeake Bay Program Water Quality Monitoring Data. Chesapeake Bay Program Retrieved from https://www.chesapeakebay.net/documents/3676/wq_data_userguide_10feb12_mod.pdf.
Fall, K.A., 2020. Influence of suspended particle size and composition on particle image processing, estuarine floc fractal properties, and resulting estuarine light attenuation. Virginia Insitute of Marine Science, William & Mary. doi:10.25773/v5-nn75-t992.
Fall, K.A., Friedrichs, C.T., Massey, G.M., Bowers, D.G., Smith, S.J., 2021. The importance of organic content to fractal floc properties in estuarine surface waters: insights from video, LISST, and pump sampling. J. Geophys. Res. Ocean. 126. https://doi.org/10.1029/2020jc016787 e2020JC016787.
Fasham, M.J.R., Ducklow, H.W., McKelvie, S.M., 1990. A nitrogen-based model of plankton dynamics in the oceanic mixed layer. J. Mar. Res. 48, 591–639. https://doi.org/10.1357/002224090784984678.
Feng, Y., Friedrichs, M.A.M., Wilkin, J., Tian, H., Yang, Q., Hofmann, E.E., Wiggert, J.D., Hood, R.R., 2015. Chesapeake Bay nitrogen fluxes derived from a land-estuarine ocean biogeochemical modeling system: Model description, evaluation, and nitrogen budgets. J. Geophys. Res. Biogeosciences 1666–1695. doi:10.1002/2015JG002931
Fennel, K., Wilkin, J., Levin, J., Moisan, J., O'Reilly, J., Haidvogel, D., 2006. Nitrogen cycling in the Middle Atlantic Bight: results from a three-dimensional model and implications for the North Atlantic nitrogen budget. Glob. Biogeochem. Cycles 20, 1–14. https://doi.org/10.1029/2005GB002456.
Fischer, G., Karakaş, G., 2009. Sinking rates and ballast composition of particles in the Atlantic ocean: implications for the organic carbon fluxes to the deep ocean. Biogeosciences 6, 85–102. https://doi.org/10.5194/bg-6-85-2009.
Fleming-Lehtinen, V., Laamanen, M., 2012. Long-term changes in Secchi depth and the role of phytoplankton in explaining light attenuation in the Baltic Sea. Estuar. Coast. Shelf Sci. 102–103, 1–10. https://doi.org/10.1016/j.ecss.2012.02.015.
Gallegos, C.L., Werdell, P.J., McClain, C.R., 2011. Long-term changes in light scattering in Chesapeake Bay inferred from Secchi depth, light attenuation, and remote sensing measurements. J. Geophys. Res. Ocean. 116, 1–19. https://doi.org/10.1029/2011JC007160.
Garcia, H.E., Gordon, L.I., 1992. Oxygen solubility in seawater: better fitting equations. Limnol. Oceanogr. 37 (6), 1307–1312. https://doi.org/10.4319/lo.1992.37.6.1307.
Gittman, R.K., Fodrie, F.J., Popowich, A.M., Keller, D.A., Bruno, J.F., Currin, C.A., Peterson, C.H., Piehler, M.F., 2015. Engineering away our natural defenses: an analysis of shoreline hardening in the US. Front. Ecol. Environ. 13, 301–307. https://doi.org/10.1890/150065.
Halka, J.P., Hopkins, K., Hardaway, S., Hennessee, E.L., Offerman, K., 2006. Shore Erosion as a Source of Estuarine Sediments: Chesapeake Bay, in: Geolologial Society of America. PA, Philadelphia, p. 2006.
Hamm, C.E., 2002. Interactive aggregation and sedimentation of diatoms and clay-sized lithogenic material. Limnol. Oceanogr. 47, 1790–1795. https://doi.org/10.4319/lo.2002.47.6.1790.
Hardaway, C.S.S., Byrne, R.J.J., 1999. Shoreline Management in Chesapeake Bay. Spec. Rep. Appl. Mar. Sci. Ocean Eng. Number 356. Virginia Sea Grant Publ. VSG-99-11 56. doi:10.21220/V5DB1X
Hardaway, C.S., Milligan, D.A., Wilcox, C.A., 2017. Shoreline Studies Program shoreline evolution database 1937–2009. Retrieved from http://www.vims.edu.
Harding, L.W., Gallegos, C.L., Perry, E.S., Miller, W.D., Adolf, J.E., Mallonee, M.E., Paerl, H.W., 2016. Long-term trends of nutrients and phytoplankton in Chesapeake Bay. Estuar. Coasts 39, 664–681. https://doi.org/10.1007/s12237-015-0023-7.
Harding, L.W., Mallonee, M.E., Perry, E.S., David Miller, W., Adolf, J.E., Gallegos, C.L., Paerl, H.W., 2020. Seasonal to inter-annual variability of primary production in Chesapeake Bay: prospects to reverse eutrophication and change trophic classification. Sci. Rep. 10, 1–20. https://doi.org/10.1038/s41598-020-58702-3.
Harris, C.K., Sherwood, C.R., Signell, R.P., Bever, A.J., Warner, J.C., 2008. Sediment dispersal in the northwestern Adriatic Sea. J. Geophys. Res. Ocean. 113, 1–18. https://doi.org/10.1029/2006JC003868.
Harvey, E.T., Walve, J., Andersson, A., Karlson, B., Kratzer, S., 2019. The effect of optical properties on secchi depth and implications for eutrophication management. Front. Mar. Sci. 5, 1–19. https://doi.org/10.3389/fmars.2018.00496.
Hernádez, C., Gocke, K., 1988. Productividad Primaria en la Cienága Grande de Santa Marta, Colombia. An. Inst. Invest. Mar. Punta Betin 19, 101–119.
Holmes, R.W., 1970. The Secchi disk in turbid coastal waters. Limnol. Oceanogr. 15, 688–694. https://doi.org/10.4319/lo.1970.15.5.0688.
Hou, W., Lee, Z., Weidemann, A.D., 2007. Why does the Secchi disk disappear? An imaging perspective. Opt. Express 15, 2791. https://doi.org/10.1364/oe.15.002791.
Irby, I.D., Friedrichs, M.A.M., 2019. Evaluating confidence in the impact of regulatory nutrient reduction on Chesapeake Bay water quality. Estuar. Coasts 42, 16–32. https://doi.org/10.1007/s12237-018-0440-5.
Irby, I., Friedrichs, M.A.M., Da, F., Hinson, K., 2018. The competing impacts of climate change and nutrient reductions on dissolved oxygen in Chesapeake Bay. Biogeosciences 15, 2649–2668. https://doi.org/10.5194/bg-15-2649-2018.
Irigoien, X., Castel, J., 1997. Light limitation and distribution of chlorophyll pigments in a highly turbid estuary: the Gironde (SW France). Estuar. Coast. Shelf Sci. 44, 507–517. https://doi.org/10.1006/ecss.1996.0132.
Isdell, R.E., 2014. Anthropogenic modifications of connectivity at the aquatic-terrestrial ecotone in the Chesapeake Bay. William & Mary. doi:10.21220/s2-pc6w-dv02.
Jassby, A.D., Reuter, J.E., Goldman, C.R., 2003. Determining long-term water quality change in the presence of climate variability: Lake Tahoe (U.S.A.). Can. J. Fish. Aquat. Sci. 60, 1452–1461. https://doi.org/10.1139/f03-127.
Johnson, E.R., Inamdar, S., Kan, J., Vargas, R., 2018. Particulate organic matter composition in stream runoff following large storms: role of POM sources, particle size, and event

characteristics. J. Geophys. Res. Biogeosci. 123, 660–675. https://doi.org/10.1002/2017JG004249.
Jones, C.M., 2014. Can we predict the future: juvenile finfish and their seagrass nurseries in the Chesapeake Bay. ICES J. Mar. Sci. 71, 681–688. https://doi.org/10.1093/icesjms/fst142.
Justić, D., 1988. Trend in the transparency of the northern Adriatic Sea 1911-1982. Mar. Pollut. Bull. 19, 32–35. https://doi.org/10.1016/0025-326X(88)90751-5.
Keisman, J., Friedrichs, C., Batiuk, R., Blomquist, J., Cornwell, J., Gallegos, C., Lyubchich, S., Moore, K., Murphy, R., Orth, R., Sanford, L., Tango, P., Testa, J., Trice, M., Zhang, Q., 2019. Understanding and explaining 30 years of water clarity trends in the Bay's tidal waters. STAC Publication Number 19–004. MD, Edgewater Retrieved from. http://www.chesapeake.org/pubs/411_Keisman2019.pdf.
Kim, G.E., St-Laurent, P., Friedrichs, M.A.M., Mannino, A., 2020. Impacts of water clarity variability on temperature and biogeochemistry in the Chesapeake Bay. Estuar. Coasts 43, 1973–1991. https://doi.org/10.1007/s12237-020-00760-x.
Kirk, J.T.O., 1994. Light and Photosynthesis in Aquatic Ecosystems. 3rd ed. Cambridge University Press, Cambridge.
Klaas, C., Archer, D.E., 2002. Association of sinking organic matter with various types of mineral ballast in the deep sea: implications for the rain ratio. Glob. Biogeochem. Cycles 16, 1–14. https://doi.org/10.1029/2001GB001765.
Klemick, H., Griffiths, C., Guignet, D., Walsh, P., 2018. Improving water quality in an iconic estuary: an internal meta-analysis of property value impacts around the Chesapeake Bay. Environ. Resour. Econ. 69, 265–292. https://doi.org/10.1007/s10640-016-0078-3.
Koenings, J.P., Edmundson, J.A., 1991. Secchi disk and photometer estimates of light regimes in Alaskan lakes: effects of yellow color and turbidity. Limnol. Oceanogr. 36, 91–105. https://doi.org/10.4319/lo.1991.36.1.0091.
Kranck, K., Milligan, T., 1980. Macroflocs: production of marine snow in the laboratory. Mar. Ecol. Prog. Ser. 3, 19–24. https://doi.org/10.3354/meps003019.
Kriest, I., 2002. Different parameterizations of marine snow in a 1D-model and their influence on representation of marine snow, nitrogen budget and sedimentation. Deep. Res. Part I Oceanogr. Res. Pap. 49, 2133–2162. https://doi.org/10.1016/S0967-0637(02)00127-9.
Kromkamp, J., Peene, J., van Rijswijk, P., Sandee, A., Goosen, N., 1995. Nutrients, light and primary production by phytoplankton and microphytobenthos in the eutrophic, turbid Westerschelde estuary (the Netherlands). Hydrobiologia 311, 9–19. https://doi.org/10.1007/BF00008567.
Lefcheck, J.S., Orth, R.J., Dennison, W.C., Wilcox, D.J., Murphy, R.R., Keisman, J., Gurbisz, C., Hannam, M., Landry, J.B., Moore, K.A., Patrick, C.J., Testa, J., Weller, D.E., Batiuk, R.A., 2018. Long-term nutrient reductions lead to the unprecedented recovery of a temperate coastal region. Proc. Natl. Acad. Sci. 115 (14), 3658–3662. https://doi.org/10.1073/pnas.1715798115.
Luettich, R.A., Westerink, J.J., Scheffner, N.W., 1992. ADCIRC: an advanced three-dimensional circulation model for shelves, coasts, and estuaries. Report 1 Theory and Methodology of ADCIRC-2DDI and ADCIRC-3DL. MS, Vicksburg Retrieved from. https://hdl.handle.net/11681/4618.
Maa, J.P.-Y., Sanford, L., Halka, J.P., 1998. Sediment resuspension characteristics in Baltimore Harbor. Maryland. Mar. Geol. 146, 137–145. https://doi.org/10.1016/S0025-3227(97)00120-5.
Madsen, O.S., 1994. Spectral Wave-Current Bottom Boundary Layer Flows, in: Proceedings of the 24th International Conference on Coastal Engineering. Coastal Engineering Research Council/ ASCE, Kobe, Japan, pp. 384–398 https://doi.org/10.9753/icce.v24.
Malpezzi, M.A., Sanford, L.P., Crump, B.C., 2013. Abundance and distribution of transparent exopolymer particles in the estuarine turbidity maximum of Chesapeake Bay. Mar. Ecol. Prog. Ser. 486, 23–35. https://doi.org/10.3354/meps10362.
Mangan, S., Lohrer, A.M., Thrush, S.F., Pilditch, C.A., 2020. Water column turbidity not sediment nutrient enrichment moderates microphytobenthic primary production. J. Mar. Sci. Eng. 8. https://doi.org/10.3390/jmse8100732.
Marshall, H.G., Lacouture, R.V., Buchanan, C., Johnson, J.M., 2006. Phytoplankton assemblages associated with water quality and salinity regions in Chesapeake Bay. USA. Estuar. Coast. Shelf Sci. 69, 10–18. https://doi.org/10.1016/j.ecss.2006.03.019.
Martin, D., Bertasi, F., Colangelo, M.A., de Vries, M., Frost, M., Hawkins, S.J., Macpherson, E., Moschella, P.S., Satta, M.P., Thompson, R.C., Ceccherelli, V.U., 2005. Ecological impact of coastal defence structures on sediment and mobile fauna: evaluating and forecasting consequences of unavoidable modifications of native habitats. Coast. Eng. 52, 1027–1051. https://doi.org/10.1016/j.coastaleng.2005.09.006.
McSweeney, J.M., Chant, R.J., Wilkin, J.L., Sommerfield, C.K., 2017. Suspended-sediment impacts on light-limited productivity in the Delaware Estuary. Estuar. Coasts 40, 977–993. https://doi.org/10.1007/s12237-016-0200-3.
Moore, M.R., Doubek, J.P., Xu, H., Cardinale, B.J., 2020. Hedonic price estimates of lake water quality: valued attribute, instrumental variables, and ecological-economic benefits. Ecol. Econ. 176, 106692. https://doi.org/10.1016/j.ecolecon.2020.106692.
Moriarty, J.M., Friedrichs, M.A.M., Harris, C.K., 2021. Seabed resuspension in the Chesapeake Bay: implications for biogeochemical cycling and hypoxia. Estuar. Coasts 44, 103–122. https://doi.org/10.1007/s12237-020-00763-8.
Murphy, R.R., Perry, E., Harcum, J., Keisman, J., 2019. A Generalized Additive Model approach to evaluating water quality: Chesapeake Bay case study. Environ. Model. Softw. 118, 1–13. https://doi.org/10.1016/j.envsoft.2019.03.027.
Nichols, M.M., Kim, S.C., Brouwer, C.M., 1991. Sediment Characterization of the Chesapeake Bay and its Tributaries, Virginian Province. doi:10.21220/V5BQ60.
Niemeyer, D., Kriest, I., Oschlies, A., 2019. The effect of marine aggregate parameterisations on nutrients and oxygen minimum zones in a global biogeochemical model. Biogeosciences 16, 3095–3111. https://doi.org/10.5194/bg-16-3095-2019.
Olesen, B., 1996. Regulation of light attenuation and eelgrass Zostera marina depth distribution in a Danish embayment. Mar. Ecol. Prog. Ser. 134, 187–194. https://doi.org/10.3354/meps134187.
Palinkas, C.M., Russ, E., 2019. Spatial and temporal patterns of sedimentation in an infilling reservoir. Catena 180, 120–131. https://doi.org/10.1016/j.catena.2019.04.024.
Passow, U., 2004. Switching perspectives: Do mineral fluxes determine particulate organic carbon fluxes or vice versa? Geochem. Geophys. Geosyst. 5 (4). https://doi.org/10.1029/2003GC000670.
Patrick, C.J., Weller, D.E., Li, X., Ryder, M., 2014. Effects of shoreline alteration and other stressors on submerged aquatic vegetation in subestuaries of Chesapeake Bay and the mid-Atlantic coastal bays. Estuar. Coasts 37, 1516–1531. https://doi.org/10.1007/s12237-014-9768-7.
Patrick, C.J., Weller, D.E., Ryder, M., 2016. The relationship between shoreline armoring and adjacent submerged aquatic vegetation in Chesapeake Bay and nearby Atlantic Coastal Bays. Estuar. Coasts 39, 158–170. https://doi.org/10.1007/s12237-015-9970-2.
Pedersen, T.M., Sand-Jensen, K., Markager, S., Nielsen, S.L., 2014. Optical changes in a eutrophic estuary during reduced nutrient loadings. Estuar. Coasts 37, 880–892. https://doi.org/10.1007/s12237-013-9732-y.
Peterson, E.L., 1999. Benthic shear stress and sediment condition. Aquac. Eng. 21, 85–111. https://doi.org/10.1016/S0144-8609(99)00025-4.
Peterson, C.H., Summerson, H.C., Thomson, E., Lenihan, H.S., Grabowski, J., Manning, L., Micheli, F., Johnson, G., 2000. Synthesis of linkages between benthic and fish communities as a key to protecting essential fish habitat. Bull. Mar. Sci. 66, 759–774.
Preisendorfer, R.W., 1986. Secchi disk science: visual optics of natural waters. Limnol. Oceanogr. 31, 909–926. https://doi.org/10.4319/lo.1986.31.5.0909.
Prosser, D.J., Jordan, T.E., Nagel, J.L., Seitz, R.D., Weller, D.E., Whigham, D.F., 2017. Impacts of coastal land use and shoreline armoring on estuarine ecosystems: an introduction to a special issue. Estuar. Coasts, 1–17 https://doi.org/10.1007/s12237-017-0331-1.
Ralston, D.K., Geyer, W.R., 2009. Episodic and long-term sediment transport capacity in The Hudson River estuary. Estuar. Coasts 32, 1130–1151. https://doi.org/10.1007/s12237-009-9206-4.
Reustle, J.W., Smee, D.L., 2020. Cloudy with a chance of mesopredator release: turbidity alleviates top-down control on intermediate predators through sensory disruption. Limnol. Oceanogr. 1–13. https://doi.org/10.1002/lno.11452.
Russ, E., Palinkas, C., 2020. Evolving sediment dynamics due to anthropogenic processes in upper Chesapeake Bay. Estuar. Coast. Shelf Sci. 235, 106596. https://doi.org/10.1016/j.ecss.2020.106596.
Sanford, L., 2008. Modeling a dynamically varying mixed sediment bed with erosion, deposition, bioturbation, consolidation, and armoring. Comput. Geosci. 34 (10), 1263–1283. https://doi.org/10.1016/j.cageo.2008.02.011.
Sanford, L.P., Gao, J., 2018. Influences of wave climate and sea level on shoreline erosion rates in the Maryland Chesapeake Bay. Estuar. Coasts 41, 19–37. https://doi.org/10.1007/s12237-017-0257-7.
Sanford, L.P., Maa, J.P.-Y., 2001. A unified erosion formulation for fine sediments. Mar. Geol. 179, 9–23. https://doi.org/10.1016/S0025-3227(01)00201-8.
Sanford, L.P., Suttles, S.E., Halka, J.P., 2001. Reconsidering the physics of the Chesapeake Bay estuarine turbidity maximum. Estuaries 24, 655–669. https://doi.org/10.2307/1352874.
Schaffler, J.J., van Montfrans, J., Jones, C.M., Orth, R.J., 2013. Fish species distribution in seagrass habitats of Chesapeake Bay are structured by abiotic and biotic factors. Mar. Coast. Fish. 5, 114–124. https://doi.org/10.1080/19425120.2013.804013.
Secchi, A., Cialdi, C.A., 1866. Sul moto ondoso del mare e sulle correnti de esso specialmente auqelle littorali. Cited ONI Transl. A-655, p. 1. Hydrogr. Off. 1955. 2nd. Ed., 258–288.
Shang, S., Lee, Z., Shi, L., Lin, G., Wei, G., Li, X., 2016. Changes in water clarity of the Bohai Sea: observations from MODIS. Remote Sens. Environ. 186, 22–31. https://doi.org/10.1016/j.rse.2016.08.020.
Shchepetkin, A.F., McWilliams, J.C., 2005. The regional oceanic modeling system (ROMS): a split-explicit, free-surface, topography-following-coordinate oceanic model. Ocean Model 9, 347–404. https://doi.org/10.1016/j.ocemod.2004.08.002.
Shenk, G.W., Linker, L.C., 2013. Development and application of the 2010 Chesapeake Bay Watershed total maximum daily load model. J. Am. Water Resour. Assoc. 49, 1042–1056. https://doi.org/10.1111/jawr.12109.
St-Laurent, P., Friedrichs, M.A.M., Najjar, R., Shadwick, E., Tian, H., Yao, Y., Stets, E., 2020. Relative impacts of global changes and regional watershed changes on the inorganic carbon balance of the Chesapeake Bay. Biogeosciences 17, 3779–3796. https://doi.org/10.5194/bg-2020-117.
Tarpley, D.R.N., Harris, C.K., Friedrichs, C.T., Sherwood, C.R., 2019. Tidal variation in cohesive sediment distribution and sensitivity to flocculation and bed consolidation in an idealized, partially mixed estuary. J. Mar. Sci. Eng. 7. https://doi.org/10.3390/jmse7100334.
Testa, J.M., Lyubchinch, V., Zhang, Q., 2019. Patterns and trends in Secchi disk depth over three decades in the Chesapeake Bay estuarine complex. Estuar. Coasts. https://doi.org/10.1007/s12237-019-00547-9.
Tian, H., Yang, Q., Najjar, R.G., Ren, W., Friedrichs, M.A.M., Hopkinson, C.S., Pan, S., 2015. Anthropogenic and climatic influences on carbon fluxes from easter North America to the Atlantic Ocean: a process-based modeling study. J. Geophys. Res. Biogeosci. 120, 752–772. https://doi.org/10.1002/2014JG002760.
Tyler, J.E., 1968. The Secchi disc. Limnol. Oceanogr. 13, 1–6. https://doi.org/10.4319/lo.1968.13.1.0001.
Walsh, P., Griffiths, C., Guignet, D., Klemick, H., 2017. Modeling the property price impact of water quality in 14 Chesapeake Bay counties. Ecol. Econ. 135, 103–113. https://doi.org/10.1016/j.ecolecon.2016.12.014.
Wang, P., Linker, L.C., Batiuk, R.A., 2013. Monitored and modeled correlations of sediment and nutrients with Chesapeake Bay water clarity. J. Am. Water Resour. Assoc. 49, 1103–1118. https://doi.org/10.1111/jawr.12104.
Wang, C., Li, W., Chen, S., Li, D., Wang, D., Liu, J., 2018. The spatial and temporal variation of total suspended solid concentration in Pearl River Estuary during 1987–2015

based on remote sensing. Sci. Total Environ. 618, 1125–1138. https://doi.org/10.1016/j.scitotenv.2017.09.196.

Whyte, J.N.C., 1987. Biochemical composition and energy content of six species of phytoplankton used in mariculture of bivalves. Aquaculture 60, 231–241. https://doi.org/10.1016/0044-8486(87)90290-0.

Williams, M.R., Filoso, S., Longstaff, B.J., Dennison, W.C., 2010. Long-term trends of water quality and biotic metrics in Chesapeake Bay: 1986 to 2008. Estuar. Coasts 33, 1279–1299. https://doi.org/10.1007/s12237-010-9333-y.

Wu, W., Perera, C., Smith, J., Sanchez, A., 2018. Critical shear stress for erosion of sand and mud mixtures. J. Hydraul. Res. 56, 96–110. https://doi.org/10.1080/00221686.2017.1300195.

Xu, J., Hood, R.R., Chao, S.-Y., 2005. A simple empirical optical model for simulating light attenuation variability in a partially mixed estuary. Estuaries 28, 572–580. https://doi.org/10.1007/BF02696068.

Xu, J., Long, W., Wiggert, J.D., Lanerolle, L.W.J., Brown, C.W., Murtugudde, R., Hood, R.R., 2012. Climate forcing and salinity variability in Chesapeake Bay, USA. Estuar. Coasts 35, 237–261. https://doi.org/10.1007/s12237-011-9423-5.

Zhang, Q., Tango, P.J., Murphy, R.R., Forsyth, M.K., Tian, R., Keisman, J., Trentacoste, E.M., 2018. Chesapeake bay dissolved oxygen criterion attainment deficit: three decades of temporal and spatial patterns. Front. Mar. Sci. 5, 1–15. https://doi.org/10.3389/fmars.2018.00422.